JEM

Article

Rab6-dependent retrograde traffic of LAT controls immune synapse formation and T cell activation

Jean-Marie Carpier,[1]* Andres E. Zucchetti,[1]* Laurence Bataille,[1]** Stéphanie Dogniaux,[1]** Massiullah Shafaq-Zadah,[3]** Sabine Bardin,[2] Marco Lucchino,[3] Mathieu Maurin,[1] Leonel D. Joannas,[1] Joao Gamelas Magalhaes,[1] Ludger Johannes,[3] Thierry Galli,[4] Bruno Goud,[2] and Claire Hivroz[1]

[1]Crosstalk between T Cells and Dendritic Cells Group, Institut Curie, Paris Sciences and Lettres Research University, INSERM U932, Paris, France
[2]Molecular Mechanisms of Intracellular Transport Group, Institut Curie, Paris Sciences and Lettres Research University, CNRS UMR 144, Paris, France
[3]Cellular and Chemical Biology of Membranes and Therapeutic Delivery Unit, Institut Curie, Paris Sciences and Lettres Research University, INSERM U1143, CNRS UMR 3666, Paris, France
[4]Center of Psychiatry and Neurosciences, Membrane Traffic in Health and Diseased Brain, Université Paris Descartes, Sorbonne Paris Cité, INSERM ERL U950, Paris, France

The adapter molecule linker for activation of T cells (LAT) orchestrates the formation of signalosomes upon T cell receptor (TCR) stimulation. LAT is present in different intracellular pools and is dynamically recruited to the immune synapse upon stimulation. However, the intracellular traffic of LAT and its function in T lymphocyte activation are ill defined. We show herein that LAT, once internalized, transits through the Golgi–trans-Golgi network (TGN), where it is repolarized to the immune synapse. This retrograde transport of LAT depends on the small GTPase Rab6 and the target soluble *N*-ethylmaleimide-sensitive factor attachment protein receptor (t-SNARE) Syntaxin-16, two regulators of the endosome-to-Golgi/TGN retrograde transport. We also show in vitro in Syntaxin-16– or Rab6-silenced human cells and in vivo in CD4$^+$ T lymphocytes of the Rab6 knockout mouse that this retrograde traffic controls TCR stimulation. These results establish that the retrograde traffic of LAT from the plasma membrane to the Golgi-TGN controls the polarized delivery of LAT at the immune synapse and T lymphocyte activation.

INTRODUCTION

T lymphocyte activation relies on the cognate recognition by the TCR of the MHC-associated peptide ligand (pMHC) presented at the surface of an APC. Engagement of the TCR induces a cascade of biochemical reactions that involves tyrosine phosphorylation of the CD3-ζ complexes by the kinase Lck and recruitment of the cytosolic tyrosine kinase ZAP70 to these phosphorylated complexes (Weiss and Littman, 1994). ZAP70 then phosphorylates multiple tyrosines in the cytoplasmic domain of the transmembrane protein LAT (for linker of activated T cells; Zhang et al., 1998). Once phosphorylated, LAT interacts with several adapter proteins and enzymes near the site of TCR engagement and forms nanostructures of multimolecular signaling complexes (Sherman et al., 2011; Roncagalli et al., 2014), which organize hierarchically (Sherman et al., 2016) and segregate from inhibitory molecules (Su et al., 2016). These complexes control downstream signaling and T lymphocyte development (Zhang et al., 1998) and activation (Samelson, 2002). This process is organized in time and space by a structure that forms at the interface between T lymphocyte and APC: the immune synapse (IS). The IS allows the long-lasting signaling required for T cell activation (Grakoui et al., 1999; Fooksman et al., 2010).

The TCR-induced signaling cascade has long been presented as a linear cascade of events taking place exclusively at the plasma membrane. However, it is now clear that TCR-induced signaling is modular and involves distinct pools of signaling molecules at the plasma membrane and in intracellular compartments (Ehrlich et al., 2002; Das et al., 2004; Yudushkin and Vale, 2010; Antón et al., 2011; Finetti et al., 2014; Bouchet et al., 2016). Along these lines, we and others have shown that the intracellular vesicular pool of signaling molecules including LAT plays a key role in T cell activation (Bonello et al., 2004; Purbhoo et al., 2010; Williamson et al., 2011; Larghi et al., 2013; Soares et al., 2013). Hence, TCR signaling is regulated by the traffic of these vesicles from and to the IS (Purbhoo, 2013; Onnis et al., 2016).

One of the key questions now relates to the origin of the vesicular pool of signaling molecules. We herein address this question for LAT.

LAT is present in two pools at steady-state: one that is close or at the plasma membrane and a pericentrosomal one (Bonello et al., 2004). Upon activation, both pools are re-

*J.-M. Carpier and A.E. Zucchetti contributed equally to this paper.

**L. Bataille, S. Dogniaux, and M. Shafaq-Zadah contributed equally to this paper.

Correspondence to Claire Hivroz: claire.hivroz@curie.fr

The Rockefeller University Press
J. Exp. Med. 2018 Vol. 215 No. 4 1245–1265
https://doi.org/10.1084/jem.20162042

cruited to the IS, and both have a role in T cell activation (Lillemeier et al., 2010; Purbhoo et al., 2010; Williamson et al., 2011; Balagopalan et al., 2013; Larghi et al., 2013). As stated, LAT is a palmitoylated integral membrane protein that traffics from the Golgi apparatus to the plasma membrane (Hundt et al., 2009). Upon TCR activation, microclusters containing LAT and SLP-76, another adapter protein that binds phosphorylated LAT, transiently associate with the TCR and undergo endocytosis (Barr et al., 2006; Balagopalan et al., 2007). This endocytosis depends on the ubiquitylation of LAT by c-Cbl (Balagopalan et al., 2011). The pericentrosomal pool of LAT has been shown to colocalize with internalized transferrin (Bonello et al., 2004), suggesting that LAT does recycle. More recently, we showed that the recruitment of LAT-containing vesicles to the TCR activation sites depends on the vesicular–soluble *N*-ethylmaleimide-sensitive factor attachment protein receptor (SNARE) VAMP7 (Larghi et al., 2013). We also showed that LAT phosphorylation, formation of the LAT signalosome, and T cell activation were controlled by this VAMP7-dependent traffic of LAT. Thus, although it is clear that LAT follows both an outward flow from centrosomal intracellular compartments to the IS and an inward flow from the periphery to recycling endosomes, the exact pathway followed by this key protein of T lymphocyte activation is still poorly defined.

The retrograde pathway allows the trafficking of proteins and lipids from endosomes to the trans-Golgi network (TGN)–Golgi complex (Bonifacino and Rojas, 2006; Johannes and Popoff, 2008). This pathway is highly conserved from yeast to mammals and involves complex machinery consisting of small GTPases, tethering factors, and SNAREs (Bonifacino and Rojas, 2006). Retrograde transport from early endosomes to the TGN was first discovered through the study of protein toxins (Mallard et al., 1998). Retrograde trafficking is tightly regulated by the retromer, a cargo sorting complex (Arighi et al., 2004; Seaman, 2004), the target SNARE (t-SNARE) membrane fusion protein Syntaxin-16 (Mallard et al., 2002), and the regulatory GTPase Rab6 (Martinez et al., 1994; Mallard et al., 2002).

Using in vitro and in vivo models, we herein identify the Syntaxin-16– and Rab6-dependent retrograde trafficking as an intracellular route used by LAT to directionally traffic to the immune synapse and demonstrate its importance for TCR-induced T cell activation.

RESULTS

LAT is mislocalized in the Golgi–TGN in the absence of VAMP7

We previously showed that the recruitment of LAT to the immune synapse depends on the vesicular SNARE VAMP7 (Larghi et al., 2013). In VAMP7-silenced Jurkat T cells forming conjugates with *Staphylococcus* enterotoxin type E (SEE)–pulsed antigen presenting cells, LAT was partially retained in intracellular compartments (Fig. S1 A) and as a consequence less recruited to the immune synapse (quantified in Fig. S1 B) than in cells expressing a control nontargeting shRNA (shC) (see silencing in Fig. S1 C). We thus analyzed the relative distribution of VAMP7 and LAT by confocal microscopy. In resting Jurkat T cells, LAT was juxtaposed with the VAMP7 compartments but was more central (Fig. 1 A). VAMP7, like in other cell types (Chaineau et al., 2009) was present in the Golgi of T cells as shown by its proximity with Rab6, a small GTPase associated with Golgi-TGN membranes (Goud et al., 1990) and with Syntaxin-16, a t-SNARE localized to the Golgi stacks (Simonsen et al., 1998; Tang et al., 1998; Fig. 1 A). As shown previously for the relative distribution of VAMP7 and LAT, LAT was juxtaposed to the Golgi compartments labeled with Rab6 or Syntaxin-16, but was more central, showing only an inconspicuous colocalization with these markers (Fig. 1 A). Thus, although VAMP7 is involved in LAT trafficking to the immune synapse, at the steady-state the central pool of LAT colocalized little with VAMP7, which was mainly present in Golgi–trans-Golgi compartments. We then studied the distribution of LAT in VAMP7-silenced Jurkat T cells. In the absence of VAMP7, the intracellular pool of LAT colocalized more with the t-SNARE Syntaxin-16 (Fig. 1 B; quantified in Fig. 1 C).

These results suggest that LAT transits through the Golgi–trans-Golgi compartments, where it is retained in the absence of VAMP7.

Purified membranes containing LAT also contain proteins involved in the retrograde transport from endosomes to the Golgi–TGN

To get a better idea of the membrane compartments containing LAT, we purify these membranes and analyze their contents using a method already described (Hivroz et al., 2017). In brief (graphic summary of the process in Fig. 2 A), we mechanically disrupted the JCAM2.5 LAT-deficient T cell line (Finco et al., 1998) expressing the chimeric mouse LAT-Twin-*Strep*-Tag (LAT-TST; Roncagalli et al., 2014). After cell disruption, membranes were submitted to a floatation iodixanol gradient, and fractions were collected from top to bottom. Fraction 3 retained our interest because it contained both the chimeric LAT-TST and VAMP7 (Fig. 2 A), which was shown to control LAT transport (Larghi et al., 2013; Fig. S1 A). We thus submitted this fraction to purification on *Strep*-Tactin Sepharose and eluted the retained material with biotin. By keeping the membranes intact, this protocol allowed the purification of molecules physically associated with the LAT-TST chimeric protein as well as of molecules present in the same membrane compartments. Nonspecific binding controls were obtained by submitting fraction 3 to "nude" Sepharose precipitation and performing elution as before. The small GTPase Rab6, a key regulator of vesicular transport from and to the Golgi, was present together with the LAT-TST only in elutions from the *Strep*-Tactin Sepharose, showing that these two proteins are associated with the same membrane compartments (Fig. 2 B). Moreover, two proteins controlling the endosome-to-Golgi–

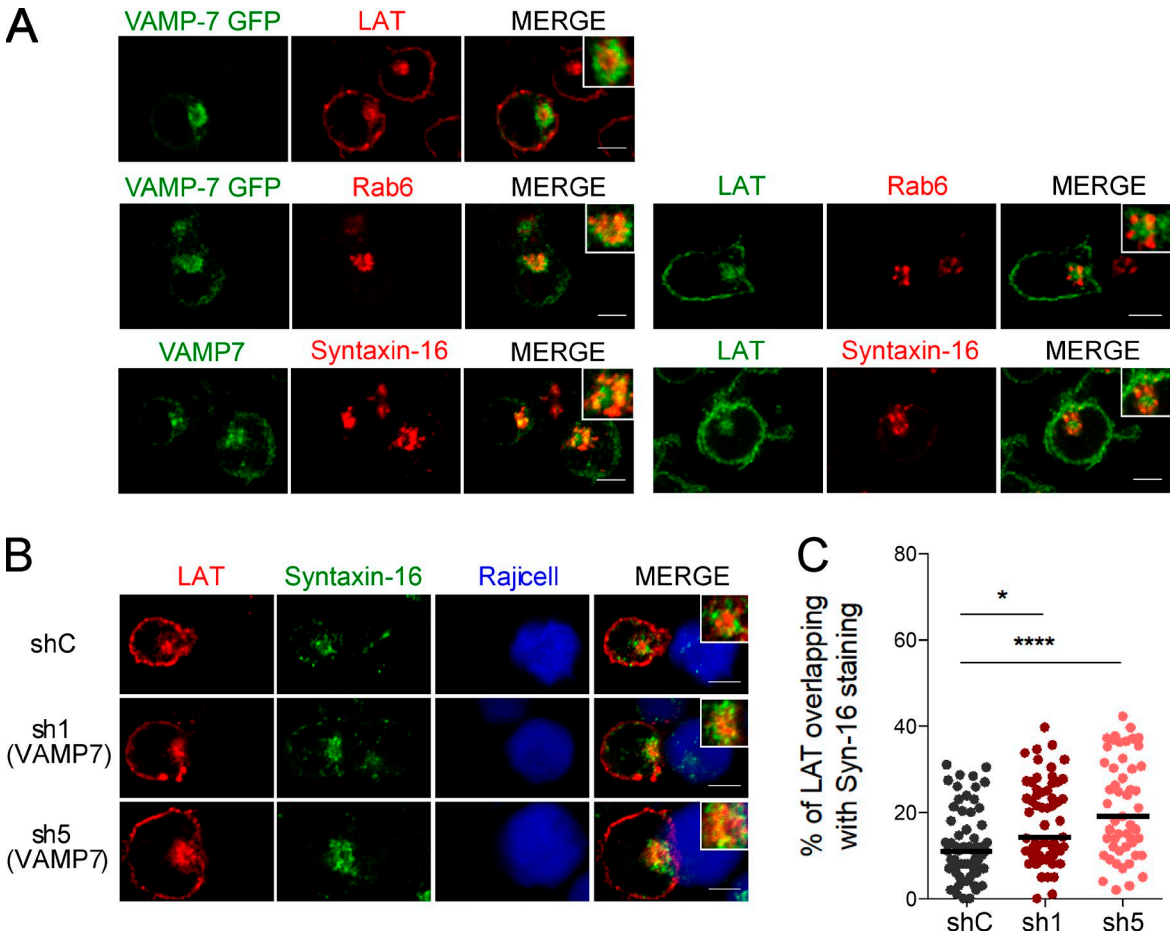

Figure 1. **LAT dynamically transits through the Golgi-TGN. (A)** Confocal images of the relative localization of VAMP7-GFP and LAT or Rab6, endogenous VAMP7 and Syntaxin-16, or LAT and Rab6 or Syntaxin-16 in Jurkat T cells. Insets show the relative localization of VAMP7, LAT, Rab6, or Syntaxin-16. Representative of two independent experiments. **(B)** Confocal images of the relative localization of LAT and Syntaxin-16 in Jurkat T cells expressing a shC or two VAMP7-targeting shRNA (sh1, sh5) in conjugates with Raji B cells. Insets show relative localization of LAT and Syntaxin-16 in control and VAMP-7–silenced Jurkat T cells. Bars, 5 µm. **(C)** Quantification of the colocalization of LAT with Syntaxin-16. Median is represented by horizontal lines. *, $P < 0.05$; ****, $P < 0.0001$ (one-way ANOVA). Data are from two independent quantifications.

trans-Golgi retrograde trafficking route, i.e., the retromer component Vps35 (Seaman et al., 1998) and the t-SNARE Syntaxin-16 (Mallard et al., 2002; Amessou et al., 2007), were also found in the eluted material, suggesting that LAT followed this transport pathway. GM130, a Golgin, LAMP1, a lysosomal membrane protein, and gp96, a chaperone of the endoplasmic reticulum, although detected in fraction 3, were absent from the eluted material, thereby establishing the specificity of the purification.

Altogether, these results suggest that LAT transits through the Golgi–trans-Golgi compartment, where it is redirected to the immune synapse.

LAT follows a Rab6/Syntaxin-16–dependent canonical retrograde transport from the plasma membrane to the Golgi-TGN, which is increased upon activation

To demonstrate that the endocytic LAT followed the retrograde transport route from the plasma membrane to the Golgi apparatus, we adapted a capture assay specifically developed to identify proteins that follow this route (Johannes and Shafaq-Zadah, 2013). To do so, plasma membrane proteins are covalently tagged with benzylguanine (BG). A capture reagent, the SNAP-tag, is fused to the Golgi membrane anchor from galactosyltransferase tagged with GFP (GalT-GFP-SNAP). After endocytosis, the BG-coupled proteins that are cargoes of the retrograde route to the Golgi-TGN are captured by the GalT-GFP-SNAP fusion protein upon formation of a covalent linkage between BG and the SNAP-tag.

In our case, Jurkat T cells expressing the HA-tagged LAT, described elsewhere (Larghi et al., 2013), were infected with a lentiviral vector encoding the GalT-GFP-SNAP (Fig. S2 A, graphical summary of the method). As reported for other cell types, the GalT-GFP-SNAP was present in the Golgi of Jurkat T cells, as shown by its colocalization with Giantin (Fig. S2 B). Moreover, it was enzymatically active because it did react with the SNAP-Cell TMR-Star, a red fluorescent sub-

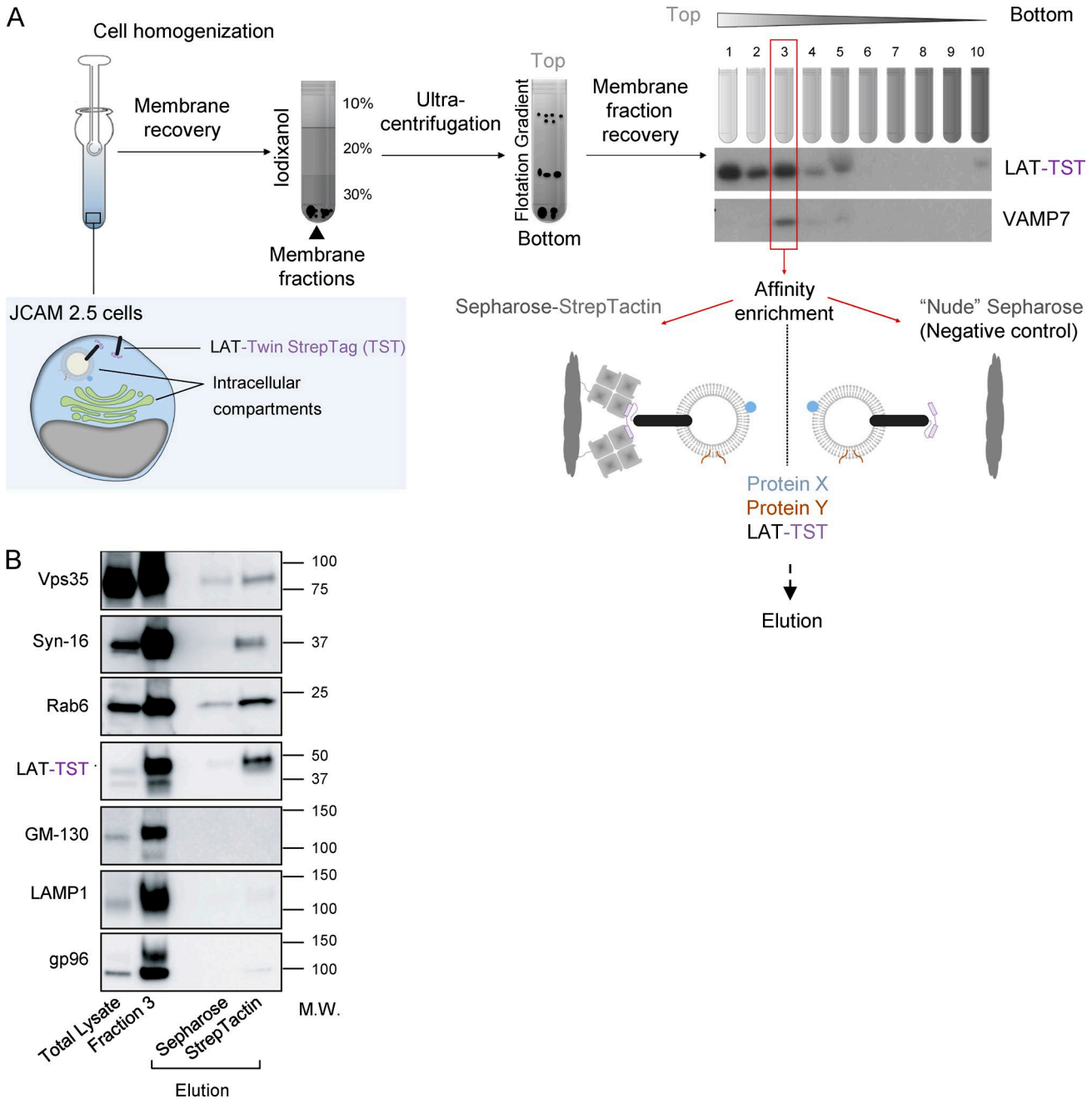

Figure 2. **LAT membranes contain proteins involved in the retrograde transport from recycling endosomes to the TGN. (A)** Schematic presentation of the purification of membranes containing LAT. JCAM2.5 LAT-deficient T cells expressing a chimeric mouse LAT-TST were mechanically disrupted. The membrane fraction was then submitted to a floatation gradient on iodixanol. After ultracentrifugation, 10 fractions from top to bottom were collected. Fraction 3 containing both the membrane associated LAT-TST and VAMP7 was mixed with *Strep*-Tactin Sepharose or uncoupled "nude" Sepharose as control. Eluted material was obtained by addition of biotin. **(B)** Western blot analysis of the eluted material. Total lysate obtained in the presence of detergent, fraction 3, or material eluted from uncoupled Sepharose or *Strep*-Tactin Sepharose were run on SDS-PAGE and immunoblotted to reveal the indicated proteins. Molecular mass is indicated in kilodaltons. Experiment representative of two independent preparations.

strate of SNAP-tag fusion proteins (Fig. S2 B). After labeling of the cell surface pool of LAT at 4°C with the anti-HA antibodies (Abs) and washing, the non-membrane permeable amino-reactive reagent BG-PEG-9-NHS was added to the medium for 45 min at 4°C. After a second wash, cells were incubated at 37°C for 4 h to allow accumulation of the endocytosed Ab-labeled HA-LAT (Fig. S2 A). Finally, after fixation, colocalization of the GalT-GFP-SNAP and of the

anti-HA was measured on confocal images. In the presence of BG-PEG-9-NHS, a colabeling between GalT-GFP-SNAP and anti-HA could clearly be detected (Fig. 3, A and B), showing that the plasma membrane pool of LAT that is constitutively endocytosed was captured in the Golgi. We then asked whether activation could increase the retrograde traffic of LAT. We thus performed the capture assay on Jurkat cells, incubated with anti-HA and BG-PEG-9-NHS as described above, which we then incubated with Raji B cells or SEE-pulsed Raji B cells for 30 min at 37°C. At this time point, no capture of the anti-HA/HA-LAT complexes was observed in Jurkat cells forming conjugates with unpulsed Raji (Fig. 3, C and D). Addition of SEE induced accumulation of the complexes in the Golgi, showing that TCR triggering increases the retrograde traffic of the endocytosed HA-LAT (Fig. 3, C and D). To formally demonstrate that LAT followed the retrograde transport from endosomes to Golgi-TGN, we silenced two proteins that play a key role in this transport process, the small GTPase Rab6 and the t-SNARE Syntaxin-16 (Mallard et al., 2002), and performed a SNAP-tag capture assay as before (see silencing, Fig. S2 C). In the presence of SEE, an accumulation of the complexes was observed in the Golgi of Jurkat T cells expressing a control shRNA. Silencing of both Rab6 and Syntaxin-16 significantly decreased the capture of the endocytosed HA-LAT in the Golgi (Fig. 3, E and F). As described, in the absence of SEE, no capture of the anti-HA/HA-LAT complexes was observed in 30-min conjugates (Fig. S2, D and E).

Altogether, these results show that the plasma membrane pool of LAT, once endocytosed, follows the retrograde route from endosome to Golgi–trans-Golgi compartment in a Rab6/Syntaxin-16–dependent manner, and that this traffic is enhanced by TCR activation.

Rab6 and Syntaxin-16 control LAT recruitment to the immune synapse and signaling in T lymphocytes

We reasoned that the retrograde traffic of LAT from the plasma membrane to the Golgi–trans-Golgi membranes might control its polarized resecretion to the immune synapse. To test this hypothesis, Rab6 or Syntaxin-16 was silenced in Jurkat cells, as before (silencing in Fig. S3 A for Rab6 and Fig. S3 C for Syntaxin-16), and endogenous LAT recruitment was analyzed by total internal reflexion fluorescence microscopy (TIRFM) in Jurkat cellsseeded on coverslips coated with anti-CD3 and anti-CD28 mAbs or poly-L-lysine as control, as previously described (Larghi et al., 2013). Upon stimulation, LAT microclusters were recruited to the immune synapse in cells expressing a control nontargeting shRNA (Fig. 4 A). In cells expressing Rab6- or Syntaxin-16–specific shRNA, LAT recruitment at the IS was decreased (Fig. 4, A and B, for Rab6; and Fig. 4, F and G, for Syntaxin-16). We also measured, in Jurkat cells expressing a chimeric CD3-ζ–GFP, the recruitment of CD3-ζ, which is also present in endocytic compartments (Blanchard et al., 2002; Yudushkin and Vale, 2010; Soares et al., 2013). In contrast to LAT, no decrease in the recruitment of CD3-ζ was observed in Rab6-silenced cells, but it was even increased in these cells (Fig. 4 C). These results suggest that the retrograde route from the plasma membrane to the Golgi apparatus is needed to polarize LAT at the IS but is not needed for CD3-ζ recruitment. Plasma membrane expression of CD3 and CD28 was not affected by Rab6 or by Syntaxin-16 silencing (Fig. S3 B for Rab6 and Fig. S3 D for Syntaxin-16). Total LAT expression was not affected, either (Fig. S3 B for Rab6 and Fig. S3 D for Syntaxin-16). Yet analysis of the different pools of LAT using the chimeric HA-LAT revealed that both Rab6 and Syntaxin-16 silencing induced an increased expression of HA-LAT at the plasma membrane for an unchanged total expression of HA-LAT (Fig. S3 E for Rab6 and Fig. S3 F for Syntaxin-16). Thus, although HA-LAT at steady-state is more expressed at the plasma membrane in Rab6 and Syntaxin-16–silenced T lymphocytes, it is less recruited at the immune synapse after 10 min of activation (Fig. 4, B and G) and less phosphorylated (Fig. 4, D, E, and I). This suggests that once endocytosed, LAT requires transport via the Rab6/Syntaxin-16–dependent retrograde pathway to be recruited back to the IS, and that this endocytic pool of LAT plays a key role in LAT signaling.

TCR-induced recruitment of LAT has been shown to precede and to be essential for phosphorylation of LAT (Williamson et al., 2011). We thus examined the phosphorylation of LAT in Jurkat cells in which Rab6 was silenced. Silenced Jurkat cells were activated with anti-CD3+CD28 Abs, and phosphorylation of LAT was analyzed by Western blot. Silencing of Rab6 was accompanied by decreased phosphorylation of LAT (Fig. 4 D and quantified in Fig. 4 E, left). In contrast, phosphorylation of the CD3-ζ chain did not show any substantial difference between control and Rab6-silencing conditions. In Syntaxin-16–silenced cells, we analyzed, by TIRFM, the phosphorylation of LAT and the recruitment of ZAP70 and its phosphorylation at the immune synapse. We showed that whereas the density of phospho-LAT microclusters was decreased in Syntaxin-16–depleted cells (Fig. 4 I), the density of ZAP70 microclusters was increased (Fig. 4 H), and that of phospho-ZAP70 microclusters (Fig. 4 J) was unchanged.

Together, these results show that Rab6 and Syntaxin-16 are required for the polarized delivery and phosphorylation of LAT at the immune synapse but are needed neither for the bulk transport to the plasma membrane nor for the induction of upstream signals such as CD3-ζ and ZAP70 recruitment and phosphorylation.

The retrograde transport machinery controls T lymphocyte functions

Jurkat cells silenced for the expression of Rab6 or Syntaxin-16 were activated for 6 h with Raji B cells pulsed with different concentrations of SEE. IL-2 present in the supernatants was measured by ELISA and was significantly decreased in both the absence of Rab6 and Syntaxin-16 (respectively, Fig. 5 A and Fig. 5 C). To discriminate between inhibition of IL-2 secretion and inhibition of IL-2 production, we measured

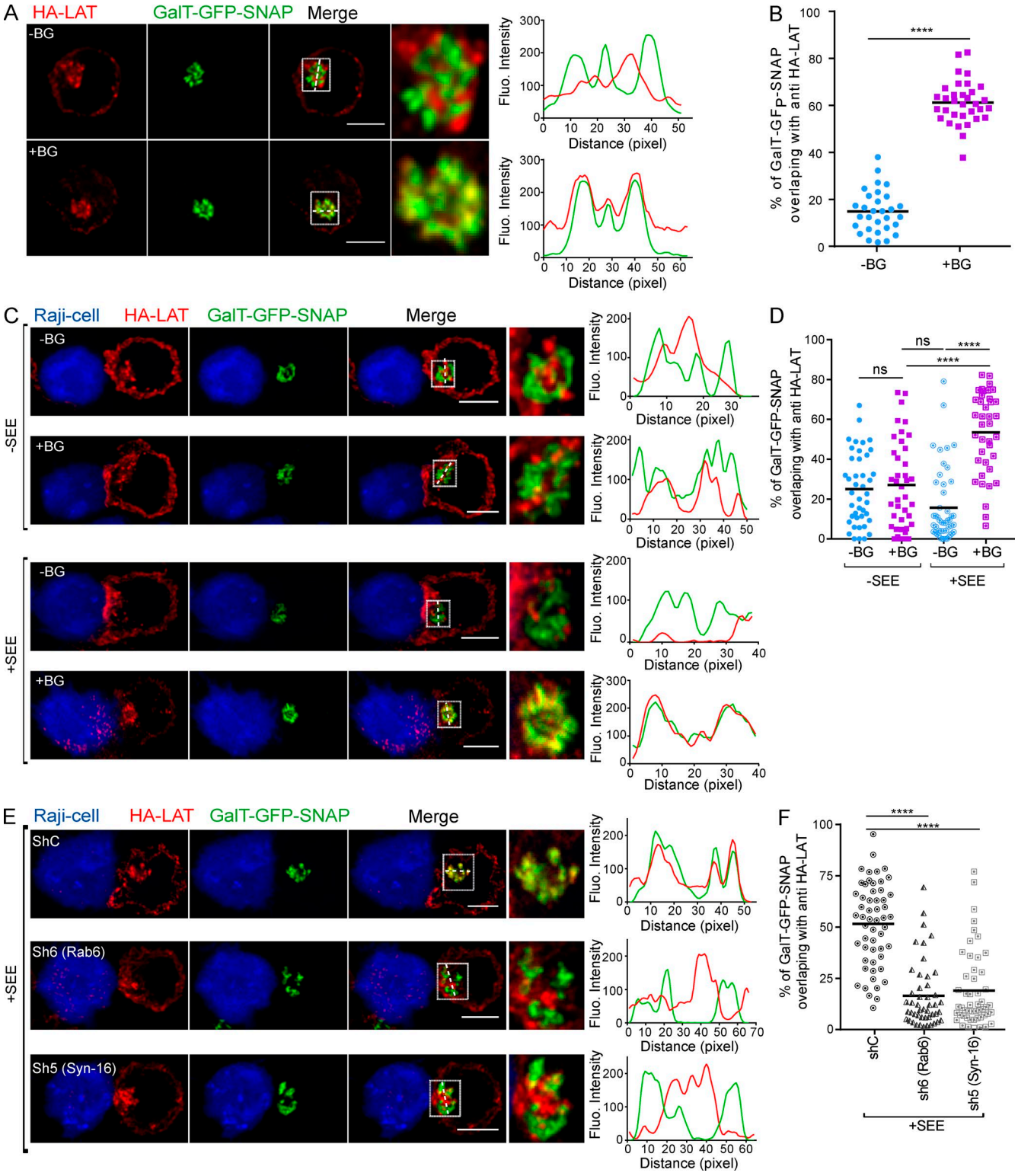

Figure 3. **LAT follows the Rab6/Syntaxin-16–dependent canonical retrograde transport from endosomes to the TGN. (A–F)** Jurkat cells expressing both GalT-GFP-SNAP and HA-LAT were incubated at 4°C with anti-HA Ab, washed, and incubated at 4°C with (+BG) or without (−BG) BG-PEG9-NHS. After washing, cells were incubated at 37°C for 4 h (A and B) or activated on slides for 30 min with Raji cells (C–F) left unpulsed (−SEE) or pulsed with SEE (+SEE). Immunolabelings were performed using anti-mouse Ig (Alexa Fluor 568) to label the anti-HA Ab and anti-GFP to label the GalT-GFP-SNAP. Colocalization of anti-HA and GalT-GFP-SNAP is shown. Quantifications show Mander's colocalization coefficient (B, D, and F). (B) Quantification of the

mRNA transcription by quantitative PCR in Rab6-silenced cells, and IL-2 production was measured by intracellular FACS in Syntaxin-16–silenced T cells (respectively, Fig. 5 B and Fig. 5 D). In both cases, IL-2 production was decreased, which showed that both Rab6 and Syntaxin-16 are involved in TCR-induced production of IL-2. An additional effect on secretion could not be excluded.

Thus, Rab6- and Syntaxin-16–dependent retrograde transport, which controls LAT delivery to the immune synapse and phosphorylation, is involved in T lymphocyte activation.

Analysis of LAT recruitment and T cell activation in Rab6-cKO T lymphocytes

To confirm the role of Rab6 in LAT recruitment and T lymphocyte activation in primary cells, mice described elsewhere (Bardin et al., 2015) in which exon 4 of *RAB6A* was flanked with *Lox*P sites were crossed with a CD4-Cre mouse line (*Rab6*$^{fl/fl}$*CD4-Cre*$^{+}$, hereafter referred as Rab6-cKO mice). As expected, Rab6 protein was depleted in CD4^{+} T cells and CD8^{+} T cells isolated from Rab6-cKO mice (not shown) but not in other tissues (Fig. 6 A). In these mice, no gross perturbation of thymic development was observed. Thymic cellularity was normal, as well as the percentage of double-negative (DN), double-positive, and single-positive (SP) CD4 and CD8 T cells (Fig. S4 A). The four stages of differentiation of the DN thymocytes (DN1, CD44^{+}CD25^{-}; DN2, CD44^{+}CD25^{+}; DN3, CD44^{-}CD25^{+}; and DN4, CD44^{-}CD25^{-}) were also normally represented in the Rab6-cKO (Fig. S4 B). In the periphery, the percentages of T lymphocytes (Fig. S4 C) CD4^{+} and CD8^{+} (Fig. S4 D), and regulatory T cells (Fig. S4 E) were also unaltered. Percentages of B lymphocytes (Fig. S4 C), CD8^{+} and CD11b^{+} dendritic cells (Fig. S4 F), and neutrophils and macrophages (Fig. S4 G) were also normal in the periphery of Rab6-cKO mice.

LAT recruitment was measured by TIRFM in isolated Rab6-cKO CD4^{+} T lymphocytes plated on coverslips coated with anti-CD3 and anti-CD28 mAbs. Rab6-cKO CD4^{+} T lymphocytes exhibited fewer LAT microclusters in the evanescent field of the TIRFM (Fig. 6 B), confirming in primary CD4^{+} T cells that Rab6 is involved in LAT recruitment to the synapse. This defect was not a result of a defect in CD3ε, CD28, or LAT expression by Rab6-cKO CD4^{+} T cells (Fig. S4 H). In contrast to LAT, the density of ZAP70 microclusters formed at the immune synapse was not altered in Rab6-cKO CD4^{+} T lymphocytes (Fig. 6 C), showing that the first events after TCR triggering are Rab6-independent.

We next tested the role of Rab6 in CD4^{+} mouse T cell activation in the context of a mixed lymphocyte reaction. Rab6-cKO and WT CD4^{+} T cells were labeled with a cell proliferation dye and incubated for 5 d with different ratios of irradiated allogeneic splenocytes as stimulatory cells (Fig. 6 D). Proliferation of Rab6-cKO T cells was significantly decreased compared with littermate controls (Fig. 6, D and E). In contrast, proliferation of Rab6-cKO T cells induced by PMA/ionomycin was unaltered (Fig. 6 G), showing that Rab6-deficient T cells can proliferate normally when activated by drugs bypassing the TCR stimulation. Moreover, the defect was T cell intrinsic and not a result of a lack of secreted factors because mixing WT and Rab6-cKO CD4^{+} T cells labeled with two different dyes did not rescue the defective proliferation of Rab6-cKO T cells (Fig. 6 F).

Thus, in primary mouse T lymphocytes, Rab6 controls LAT delivery to the immune synapse and T lymphocyte activation, confirming our previous results obtained in the Jurkat T cell line.

In vivo T lymphocyte response is abrogated in the absence of Rab6

To further document the role of Rab6 in T lymphocyte activation, we analyzed T lymphocyte responses in vivo. To do so, we first checked basal activation states of CD4^{+} T cells in the sanitary context of our animal facility. Compared with WT littermate controls, the proportion of naive CD4^{+} T cells (CD62L^{+} CD44^{-}) was significantly increased in the spleen, bone marrow (BM), and blood of Rab6 cKO mice, whereas effector/memory (CD62^{-}CD44^{+}) T cells were decreased (Fig. 7, A and B). This defect might reflect a defect in the generation or in the maintenance of memory T cells. To check if priming of T cells was altered in the absence of Rab6, we challenged the mice for a specific antigen in a polyclonal T lymphocyte context. To do so, cohorts of BM chimeras constituted of irradiated Rag2KO mice injected with BM from Rab6 cKO or WT littermate control mice were generated (experimental setup in Fig. S5 A). After 8–10 wk of reconstitution, the B and T cell compartments were comparable in both groups of mice as shown by flow cytometry analysis of the blood of chimeras (Fig. S5 B). Mice were then challenged by subcutaneous injection with OVA protein emulsified with CFA. At day 11 after injection, spleens and draining lymph nodes (LNs) were restimulated for 24 h ex vivo with a nonrelevant antigen (human serum albumin [HSA]), OVA protein class I ($OVA_{257-264}$), or class II ($OVA_{323-339}$) peptides, and the IFN-γ response was assessed by ELISPOT (Fig. 7 C). As expected, WT chimeric mice robustly responded to OVA/CFA challenge compared with mice injected with OVA alone. This response was antigen-specific given that irrelevant

colocalization after 4 h of antibody uptake. (D) Quantification compare colocalization in cells stimulated for 30 min with unpulsed or SEE-pulsed Raji B cells. (F) Quantification of the colocalization in Jurkat T cells, expressing a control (ShC), Rab6-specific (Sh6), or Syntaxin-16–specific shRNA (Sh5), activated with SEE-pulsed Raji B cells. Images show the maximum intensity from z-projections of three to five z-stacks covering the Golgi apparatus. Insets show the Golgi compartment. The profile plots of RGB images from ImageJ are shown. Means, $n = 3$ (A and B), 2 (C and D), and 2 (E and F) independent experiments for each condition. Bars, 5 µm. ****, $P < 0.0001$. (B) Student's *t* test. (D and F) One-way ANOVA.

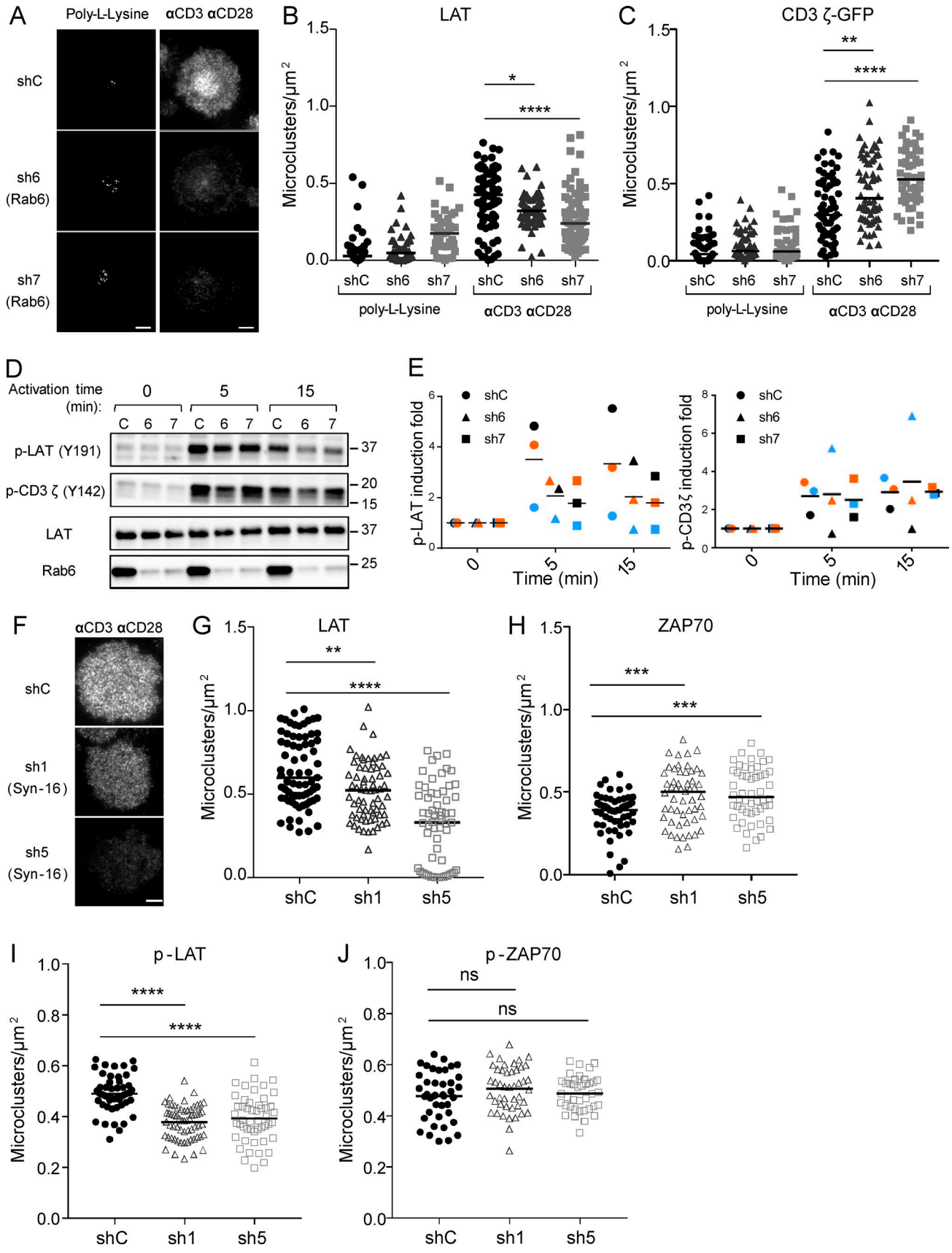

protein restimulation (HSA) did not induce an IFN-γ response (Fig. 7, C and D). In contrast, Rab6 cKO splenocytes showed a much-reduced IFN-γ response (Fig. 7, C and D). This was a global defect because IL-17A (Fig. 7, C and E), IL-2, IL-4, and IL-5 responses (Fig. S5, C–E) were abolished. Of note, PMA/ionomycin restimulation of WT and Rab6 cKO splenocytes induced similar responses (Fig. 7, D and E), indicating that Rab6-deficient $CD4^+$ T cells secreted a normal amount of cytokines when TCR triggering was bypassed. These results thus establish an important role of Rab6 in T lymphocyte activation in vivo.

Altogether, our in vivo results show that Rab6, which controls LAT retrograde traffic, plays a key role in T lymphocyte activation.

DISCUSSION

LAT is localized at the plasma membrane and in intracellular vesicles in T lymphocytes (Bonello et al., 2004). The relative contribution of each pool to the formation of microclusters found at the immune synapse and to activation of T cells is still unknown. Following up on the demonstration that the vesicular pool of LAT plays a critical role in T cell activation (Purbhoo et al., 2010; Williamson et al., 2011; Larghi et al., 2013; Soares et al., 2013), we here demonstrate that LAT traffics via the canonical Rab6/Syntaxin-16 retrograde route from the plasma membrane to the Golgi-TGN before being resecreted to the immune synapse. Our results also show that this retrograde trafficking is of critical importance for T lymphocyte activation both in vitro and in vivo.

Indeed, membranes containing LAT also contain key molecules involved in the retrograde transport of cargoes from endosomes to the Golgi–trans-Golgi such as Rab6 and Syntaxin-16 (Fig. 2). Moreover, LAT, after being endocytosed from the plasma membrane, is routed to the Golgi (Fig. 3), and this transport is blocked by silencing of Rab6 or Syntaxin-16 expression, two molecules involved in the canonical early/recycling endosomes to Golgi-TGN retrograde transport (Mallard et al., 2002). Interestingly, this retrograde transport is increased upon TCR activation, raising the question of the signaling machinery involved in this regulation. We show herein that at relatively late time point after activation (10 min), this endosome to Golgi retrograde transport of LAT is necessary to the formation of LAT microclusters at the immune synapse (Fig. 4), whereas it does not affect the recruitment of CD3-ζ. Because CD3-ζ is also present in endocytic compartments (Blanchard et al., 2002; Yudushkin and Vale, 2010; Soares et al., 2013), these results show that the endosome to Golgi retrograde transport does not apply to all the endocytosed signaling molecules involved in T cell activation. Our results also show that TCR signaling upstream of LAT recruitment was preserved as reflected by the normal phosphorylation of the CD3-ζ chain in Rab6-silenced Jurkat cells (Fig. 4) and normal density, at the immune synapse, of ZAP70 and phospho-ZAP70 in Syntaxin-16–depleted Jurkat T cells (Fig. 4) and ZAP70 in Rab6 KO $CD4^+$ mouse T cells (Fig. 6). A more thorough analysis would be required to find out if other signaling molecules are affected by the inhibition of the retrograde transport.

It is worth noting that the decreased microcluster density and phosphorylation of LAT at the immune synapse is not a result of a decreased expression of LAT at the plasma membrane. Rather, silencing of Rab6 or Syntaxin-16 both increase LAT expression at the plasma membrane without altering total LAT expression (Fig. S3). These results demonstrate that LAT neosynthesis is affected by neither Rab6 nor Syntaxin-16 silencing. They probably reflect the fact that altering one step of the very dynamic traffic of a molecule can induce an imbalanced distribution of this molecule. These results also reinforce data obtained by others and us showing that the plasma membrane pool of LAT is not the only pool contributing to LAT accumulation at the immune synapse and LAT signaling (Bonello et al., 2004; Purbhoo et al., 2010; Williamson et al., 2011; Larghi et al., 2013; Soares et al., 2013). Yet in our study, formation of the microclusters and phosphorylation of LAT are not completely abolished. This leaves some space for a contribution of the plasma membrane pool of LAT to T cell activation that has been demonstrated (Balagopalan et al., 2013). It would be interesting to kinetically follow the formation of LAT microclusters in these conditions. The reduced formation of microclusters at the immune synapse is accompanied by a defective TCR-induced IL-2 production in T cells silenced for Syntaxin-16 or Rab6 (Fig. 5), and to strongly diminished mixed lymphocyte reactions (Fig. 6) and antigenic responses in T lymphocytes from Rab6 KO mice (Fig. 7). It is worth noting that although partial, the signaling defect induces an important functional T cell defect in vivo.

Figure 4. **Rab6 and Syntaxin-16 control LAT microcluster formation at the immune synapse and LAT phosphorylation. (A)** TIRFM images of endogenous LAT in Jurkat cells expressing shC or Rab6-specific shRNA (sh6, sh7), incubated for 10 min on coverslips coated with poly-L-lysine alone (resting conditions) or anti-CD3ε+antiCD28 Abs (αCD3αCD28, activating conditions) before fixation and staining. **(B)** Quantification, in the evanescent field, of the density of LAT microclusters in Jurkat cells or **(C)** CD3ζ-GFP in Jurkat cells expressing CD3ζ-GFP. **(D)** Immunoblot analysis of phospho-LAT, phospho-CD3ζ, total LAT, and Rab6 in Jurkat cells expressing the different shRNA and activated for different times with anti-CD3ε+antiCD28 Abs. **(E)** Quantification of phospho-LAT and phospho-CD3ζ intensities, normalized on loading control, and expressed as fold increase of intensity at time 0. **(F)** TIRFM images of LAT in Jurkat cells expressing shC or Syntaxin-16–specific shRNA (sh1, sh5). **(G–J)** Quantification of the density of microclusters of LAT (G), ZAP70 (H), phospho-LAT (I), and phospho-ZAP-70 (J) in Jurkat cells, expressing control and Syntaxin-16–specific shRNA, activated for 10 min on coverslips coated with anti-CD3ε+antiCD28 Abs. *, $P < 0.05$; **, $P < 0.01$; ***, $P < 0.001$; ****, $P < 0.0001$ (one-way ANOVA). Median is represented by horizontal lines except in E, where mean is presented. All data are from two independent experiments, except for A, B and G, three independent experiments, and in E, three independent experiments each represented by one color. Bars, 5 µm.

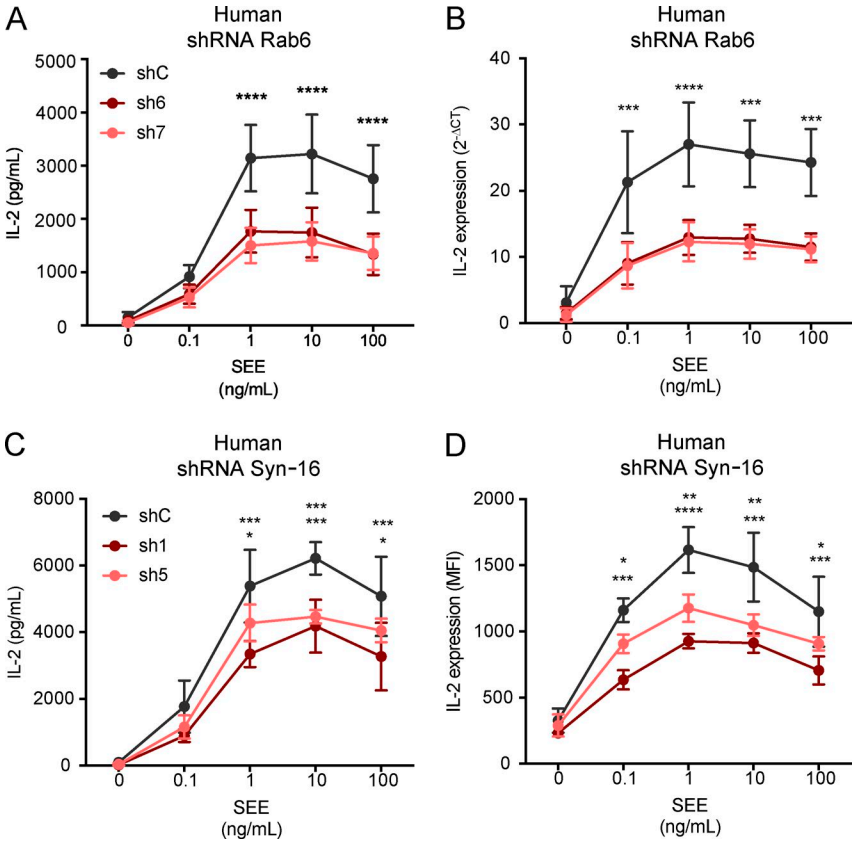

Figure 5. **Rab6 and Syntaxin-16 are required for TCR-induced IL-2 production by T lymphocytes. (A–D)** IL-2 production was measured in Jurkat cells activated for 6 h with Raji cells pulsed with different concentrations of SEE. (A and B) In cells expressing control or Rab6-specific shRNA, IL-2 in the supernatant (ELISA; A) or quantitative PCR of IL-2–specific cDNA (B). (C and D) In cells expressing control or Syntaxin-16–specific shRNA, IL-2 in supernatant (ELISA; C) or produced inside the cells (intracellular flow cytometry; D). *, $P < 0.05$; **, $P < 0.01$; ***, $P < 0.001$; ****, $P < 0.0001$ (two-way ANOVA; mean and SEM). Data represent five experiments (A), four experiments (B), and three experiments (C and D).

Rab6 deficiency results in a decreased number of memory T cells, and a defect in the production of all the cytokines tested, including Th1, Th2, and Th17 cytokines (Fig. 7 and Fig. S5), further supporting an impaired ability of $CD4^+$ T cells from *Rab6*$^{fl/fl}$ *CD4-Cre*$^+$ mice to respond to TCR signaling. These defects are not accompanied by gross defects in T cell development (Fig. S4, A and B), unlike LAT-deficient mice, which show a severe defect in intrathymic T cell development (Zhang et al., 1999). This may be a result of the fact that in $CD4^+$ T cells from *Rab6*$^{fl/fl}$/*CD4*^{Cre} mice, LAT-dependent signaling is not completely absent. Moreover, our data do not rule out a faulty maturation of T cells in the thymus that would require further analysis to be revealed.

We cannot totally exclude that diminished expressions of Rab6 and Syntaxin-16 have other effects than the mere recruitment of LAT at the immune synapse. Yet T cell activation by PMA and ionomycin of Rab6-deficient T cells was preserved (Figs. 6 and 7), showing that signaling downstream of PKC stimulation and Ca^{2+} increase does not require Rab6.

The retrograde endosome to Golgi pathway ensures several functions. First, retrograde transport can avoid the cargoes following this route from being degraded in lysosomal compartments (Lu and Hong, 2014). This might apply to LAT because upon TCR activation this molecule is ubiquitinated (Brignatz et al., 2005; Balagopalan et al., 2007; Xie et al., 2013) and degraded in a compartment, yet to be identified. However, we did not observe any decrease in LAT expression in activated T lymphocytes in which retrograde transport was inhibited (not shown).

Second and nonexclusively, the retrograde endosome to Golgi–trans-Golgi pathway can ensure the polarized "re"-secretion of recycling molecules by collecting them back in the Golgi apparatus. In other words, LAT that reaches the Golgi–trans-Golgi membrane after retrograde trafficking from the plasma membrane could then be packaged into newly formed secretory vesicles for polarized secretion from the Golgi–trans-Golgi to the immune synapse (see Fig. 8 for schematic representation of the model). Indeed, this trafficking pathway has been shown in other cell types to regulate polarized signaling by allowing proteins that follow the retrograde route to be secreted in a polarized manner to specific subdomains of the plasma membrane. This has been documented for the transmembrane protein Crumbs, which in epithelial cells recycles from endosomes to the TGN and contributes to the apical-basal polarity of these cells (Pocha et al., 2011; Zhou et al., 2011). This has also been shown for the β1 integrin that traffics in a Syntaxin-16– and Rab6-dependent manner from the plasma membrane to the TGN before being secreted in a polarized manner to the leading edge of migratory cells, allowing for persistent cell migration and efficient adhesion (Shafaq-Zadah et al., 2016). In T cells, retrograde transport of LAT back to the Golgi apparatus, which is polar-

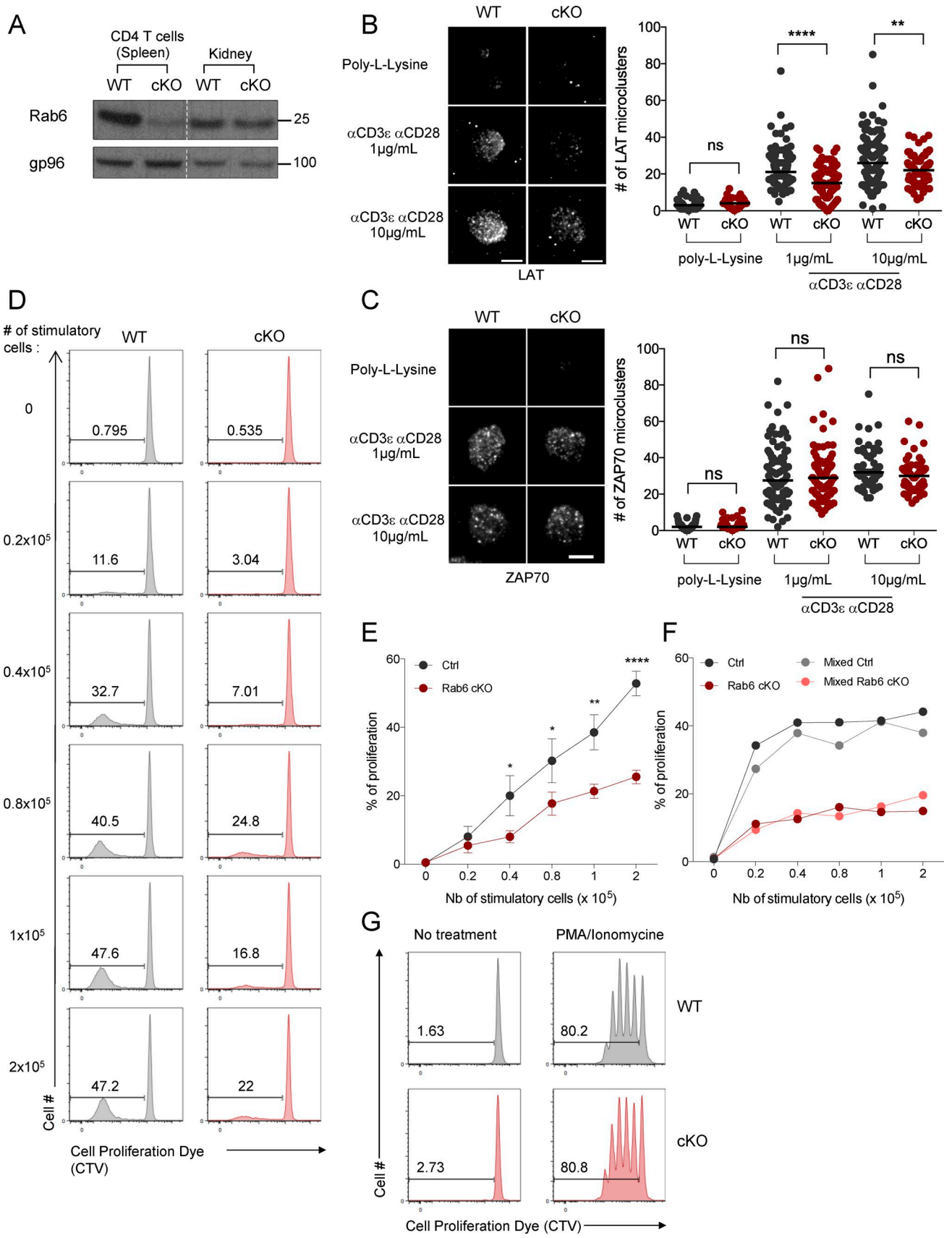

ized toward the immune synapse (Kupfer et al., 1983; Stinchcombe et al., 2006; Chemin et al., 2012), would ensure the directional delivery of recycled pools of LAT back to the immune synapse. It would also allow the recycling pool of LAT to meet again the Golgi–trans-Golgi localized VAMP7 (Fig. 1 C), which is necessary for LAT transport to the TCR activation site (Larghi et al., 2013) and more generally for the transport of vesicles from the center to the periphery of cells (Burgo et al., 2012).

Third, LAT transport to the Golgi apparatus may allow signaling in this compartment (Mayinger, 2011). Indeed, compartmentalized activation of Ras/MAPK in T lymphocytes has been reported (Bivona et al., 2003; Daniels et al., 2006; Zou et al., 2015).

We recently showed that the intraflagellar transport protein IFT20 controls LAT recruitment to the immune synapse (Vivar et al., 2016). Of note, this protein, which is involved in immune synapse (Finetti et al., 2009, 2014) and cilium formation (Follit et al., 2006) is strongly associated with the Golgi complex (Follit et al., 2008), pointing once again at the Golgi as a major hub of LAT traffic. It would be interesting to study if the Golgi localization of IFT20 is required for LAT traffic and T cell activation. By regulating the recycling of LAT at the immune synapse, the retrograde transport could define the amount of LAT available for LAT signalosome formation, providing an efficient mechanism to fine-tune signaling in T lymphocytes. This could be particularly important when T lymphocytes are activated by a low amount of MHC-peptide or weak agonists.

In conclusion, we propose herein a model in which retrograde transport from endosomes to the Golgi apparatus controls the polarized "re"-secretion of the recycling pool of LAT to the immune synapse, ensuring a sustained supply of signaling molecules and full T lymphocyte activation.

MATERIALS AND METHODS

Cells and mice

Jurkat T cells (clone E6.1), JCAM2.5 cells stably expressing the mouse LAT-TST construct (Roncagalli et al., 2014), Jurkat expressing the CD3ζ-GFP chimera described elsewhere (Blanchard et al., 2002), and Raji B cells were cultured at 37°C 5% CO_2 in RPMI 1640 GlutaMAX (Gibco-BRL 61870–010; Gibco) supplemented with 10% FCS (DE14-801F, lot 0SB017; Lonza) and were passed every 2–3 d at ∼0.5 × 10^6 cells/ml.

The Rab6 mouse strain (Bardin et al., 2015) was backcrossed more than 10 generations on a C57BL/6J background. Detection of *LoxP* sites siding exon 4 of Rab6a/a′ gene was performed by PCR using the forward primer 5′-TTGCCTCCCTGTTTGTACCAGTACGCT-3′ and reverse primer 5′-CTTCAACACAAGCCATGAAGGATC TGG-3′. To reach the excision of the exon 4 of Rab6 gene in T lymphocytes, $Rab6^{fl/fl}$ mice were crossed with transgenic CD4-Cre mouse line. $Rab6^{fl/fl}$ CD4-Cre^+ (Rab6-cKO mice) and $Rab6^{wt/wt}$ CD4-Cre^+ littermate controls (control mice) were used for experiments. Both males and females were used and matched within each experiment. Organs (spleen, thymus, LNs, mesenteric LNs [mLNs], BM) from mice were disrupted, and filtered to obtain single-cell suspensions. $CD4^+$T cells were negatively isolated from spleens and/or LNs with a Miltenyi kit (130–104-454; Miltenyi Biotec), and purity reached 95% mean. Mouse T cells were cultured in RPMI GlutaMAX supplemented with 10% FCS, 1% penicillin/streptomycin (Gibco-BRL 15–140-122; Gibco), 10 mM Hepes (Gibco-BRL 15630–080; Gibco), 1% nonessential amino acids (Gibco-BRL 11140–050; Gibco), 1 mM sodium pyruvate (Gibco-BRL 11360–070; Gibco), and 0.05 mM β-mercaptoethanol (Gibco-BRL 31350–010; Gibco) at 37°C, 5% CO_2.

BALB/cByJ mice were purchased from Charles River Laboratories, and Rag2KO mice and CD4-Cre mice were bred in our animal facility. Irradiations of cells and mice were performed with an x-ray irradiator (Philips 320 kV), and times of exposure were calculated according to periodic dosimetry in order to reach the given irradiation doses. Mouse in vivo studies were ethically approved by the French "Ministère de l'Education Nationale et de l'Enseignement supérieur" governmental committee (approval number, 05301.03).

Reagents and antibodies

For Jurkat and primary $CD4^+$ T cell activation, anti–human activating antibodies, anti-CD3ε (clone OKT3, 10 µg/ml, 16–0037-85; eBioscience) and α-CD28 (clone CD28.2, 10 µg/ml, 302923; Biolegend), and recombi-

Figure 6. **LAT recruitment to the immune synapse and late T cell activation are deficient in Rab6 cKO $CD4^+$ T lymphocytes. (A)** Immunoblot analysis of Rab6 and gp96 (loading control) expression in $CD4^+$ T cells (left) or total kidney cells (right) isolated from control (WT) and Rab6 cKO mice. Molecular mass is indicated in kilodaltons. **(B and C)** Quantification by TIRFM of the number of LAT (B) or ZAP70 (C) microclusters recruited to the immune synapse in $CD4^+$ T cells incubated on poly-L-lysine alone or anti-CD3+anti-CD28 mAb (1 or 10 µg/ml). Bars, 5 µm. **(D–F)** Flow cytometry analysis of the proliferation of $CD4^+$ T cells isolated from control (Ctrl) or Rab6 cKO mice labeled with CTV proliferation dye and stimulated for 5 d by different numbers of irradiated allogeneic Balb/C splenocytes (stimulatory cells) in a mixed lymphocyte reaction. (D) Representative experiment. (E) Percentages of proliferating $CD4^+$ T cells from five Rab6 cKO or control mice. (F) Rab6-deficient $CD4^+$ T cells labeled with the CFSE proliferation dye were either left alone (dark colors) or mixed with (1:1) control $CD4^+$ T cells labeled with CTV (light colors). Analysis of the percentages of proliferating $CD4^+$ T cells exposed for 5 d to different numbers of irradiated allogeneic Balb/C splenocytes was performed as in D. **(G)** Percentages of proliferating $CD4^+$ T cells isolated from control or Rab6 cKO mice left untreated (left) or stimulated for 5 d with low concentrations of PMA/ionomycin (7.5×10^{-7} M and 2×10^{-8} M; right). *, $P < 0.05$; **, $P < 0.01$; ****, $P < 0.0001$; one-way ANOVA in B and C; two-way ANOVA in E; mean and SEM in D. Horizontal lines represent median in B and C. Data from three experiments in B, from two experiments in C, and from four experiments in E. Data representative from three experiments in A, four in D, two in F, and three in G.

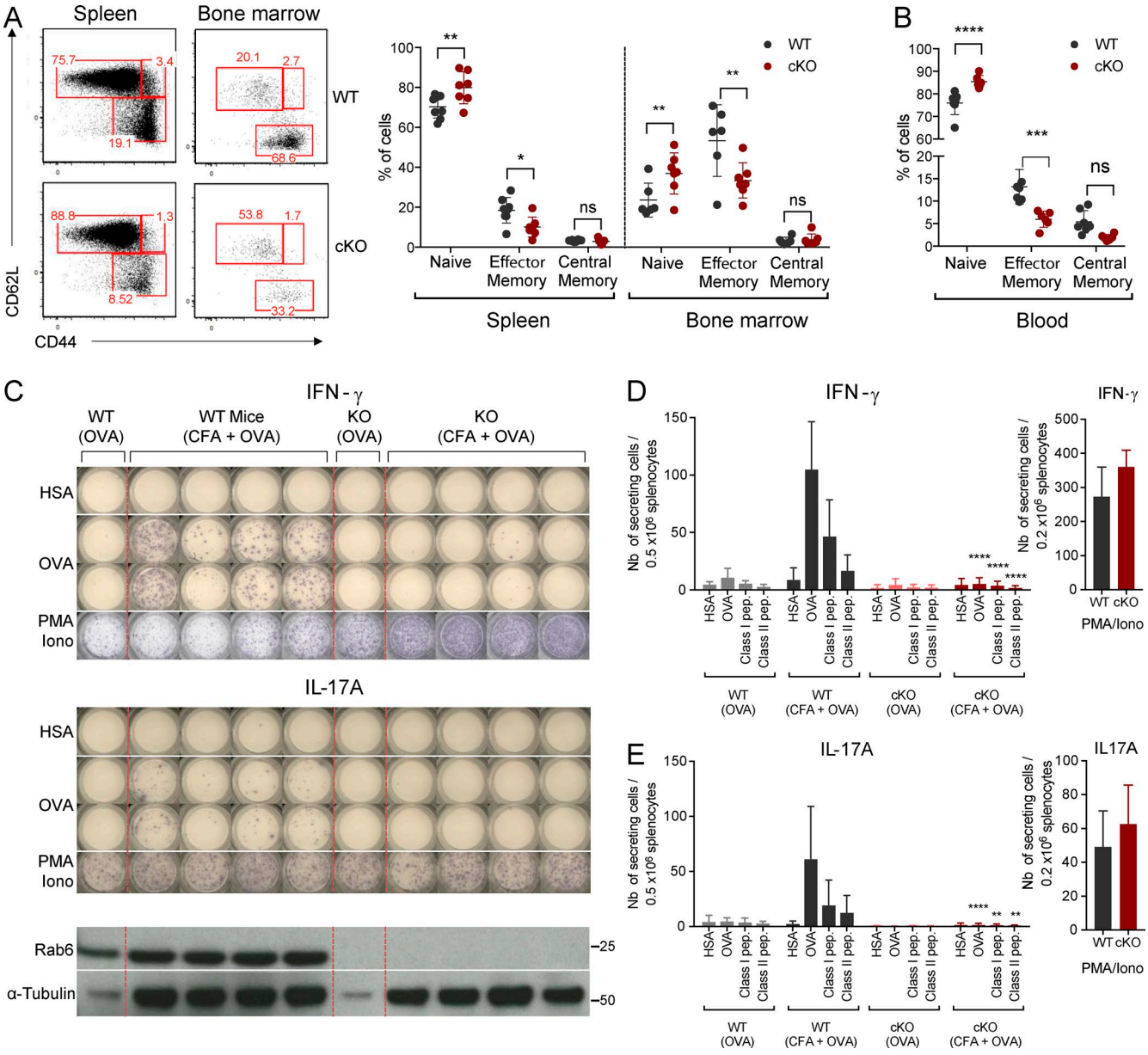

Figure 7. **T lymphocyte response in vivo is abrogated in the absence of Rab6. (A)** Representative flow cytometry analysis of naive ($CD62L^+CD44^-$), central/memory ($CD62L^+CD44^+$), and effector/memory ($CD62L^-CD44^+$) $CD4^+$ T cells in spleen and BM (left) from Rab6 cKO and control WT mice and percentages of these subpopulations (left). **(B)** Percentages of naive, central/memory, and effector/memory $CD4^+$ T cells in the blood of Rab6 cKO and control WT mice. **(C)** Representative ELISPOT analysis of the IFN-γ (top) and IL-17A (middle) responses after immunization. Splenocytes from control or Rab6 cKO bone-marrow chimeras, immunized 11 d before with OVA or CFA+OVA, were restimulated in vitro for 24 h with HSA (irrelevant antigen), OVA, or PMA/ionomycin. Each column represents one immunized mouse. Rab6 and α-tubulin expressions in $CD4^+$ T cells isolated from LNs of the same mice are shown at the bottom. **(D and E)** Quantification by ELISPOT of IFN-γ– (D) or IL-17A– (E) secreting cells from splenocytes of mice immunized as before and restimulated with HSA, OVA, MHC Class-I and MHC Class-II OVA peptides (left) or PMA/ionomycin (right; WT-OVA, $n = 3$ mice; WT CFA/OVA, $n = 13$; cKO-OVA, $n = 3$; cKO-CFA/OVA, $n = 13$). Each symbol represents a mouse (A and B). *, $P < 0.05$; **, $P < 0.01$; ***, $P < 0.001$; ****, $P < 0.0001$ (two-way ANOVA). Data represent three independent experiments (C–E; mean and SD) and one experiment (B; mean and SD).

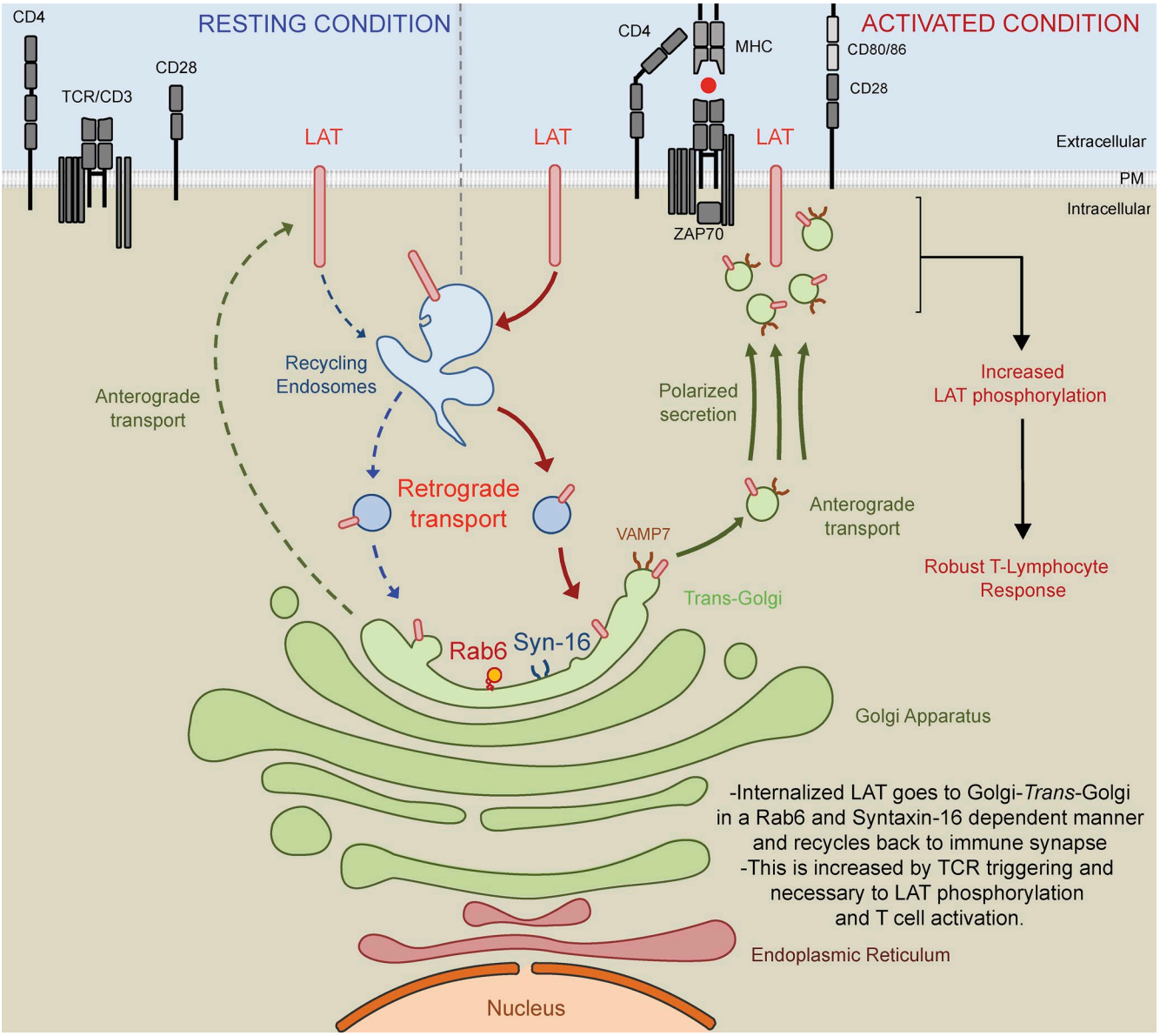

Figure 8. **Schematic representation: LAT is internalized in early/recycling endosomes and traffics back to the immune synapse through a Rab6- and Syntaxin-16–dependent endosomes to Golgi–trans-Golgi retrograde pathway.** LAT constitutively recycles from the plasma membrane to early/recycling endosomes. Our data suggest that vesicles from this compartment undergo a retrograde transport to the Golgi apparatus, which is increased upon TCR activation. Rab6 and Syntaxin-16, which play a key role in endosomes to Golgi–trans-Golgi retrograde pathway, are required for the resecretion of LAT containing vesicles to the immune synapse. Indeed, in the absence of these two molecules, LAT is not recruited to the immune synapse. We propose that this retrograde pathway allows the recycling pool of LAT to meet the VAMP7 vesicular SNARE present in the Golgi–trans-Golgi membranes, which is necessary for the polarized transport of LAT to the TCR activation site. This polarized secretion of LAT and perhaps of other molecules controlled by the endosomes to Golgi–trans-Golgi retrograde route plays a key role in T cell activation as shown by the defective TCR stimulation of T lymphocytes lacking Rab6 and Syntaxin-16.

nant SEE (MBS1112600; Cellgenetech) were used. For mouse T lymphocyte activation, anti-CD3ε (clone 145-2C11, 553057; BD Biosciences), anti-CD28 (clone 37.51, 553294; BD Biosciences), PMA (79346; Sigma-Aldrich), and ionomycin (407950; Calbiochem) were used at indicated concentrations.

Production of lentiviruses and infection of Jurkat cells

Nonreplicative VSV-g pseudotyped lentiviral particles were produced by transfecting HEK-293T cells with Gag, Pol, rev, encoding plasmid (pPAX2), envelop encoding plasmid (pMD2.G), and either the HA-Tev-LAT construct (Larghi et al., 2013) encoded in a pWXLD vector, or the SNAP-GalT-

GFP construct (Johannes and Shafaq-Zadah, 2013) encoded in a pCDH-EF1-MCS-IRES-Puro vector (SBI System Biosciences), or shRNA sequences encoded in pLKO.1 plasmid. shC (Mission shRNA SHC002; Sigma-Aldrich), VAMP7-specific shRNA, sh1 (Mission shRNA, TRCN0000059888; Sigma-Aldrich) and sh5 (Mission shRNA, TRCN0000059892; Sigma-Aldrich), Rab6a/a′-specific shRNA, sh6 (Mission shRNA, TRCN0000379588; Sigma-Aldrich) and sh7 (Mission shRNA, TRCN0000379794; Sigma-Aldrich) and Syntaxin-16–specific shRNA, sh1 (Mission shRNA, TRCN0000229991; Sigma-Aldrich), and sh5 (Mission shRNA, TRCN0000161930; Sigma-Aldrich) were used. Lentivirus were recovered in supernatant after 2 d and concentrated. 5×10^6 Jurkat T cells were infected for 24 h, when silenced cells were selected in puromycine (2 µg/ml; Invivogen) and used 5 d after infection.

Plasmids and transfection

Plasmid encoding the GFP-VAMP7 chimeric molecule was described elsewhere: (Martinez-Arca et al., 2000). 10×10^6/500 µl cells were washed and resuspended in RPMI without FCS and were electroporated, with 20 µg of the plasmid, in 4-mm gap electroporation cuvettes (5540–11; Molecular BioProducts) with a Gene Pulser electroporator (960 µF, 0.26 V; Biorad). Cells were recovered and diluted in warmed RPMI supplemented with 10% FCS and cultured for 24 h at 37°C, 5% CO_2.

Activation of Jurkat T cells for phospho-blot analysis

Jurkat T cells were activated in RPMI at 10^7 cells/ml with anti-CD3 and anti-CD28 antibodies each used at 10 µg/ml. After activation, cells were put on ice in order to stop the activation, centrifuged at 1,800 *g* at 4°C, and incubated on ice for 20 min in 30 µl of ice-cold lysis buffer (50 mM Tris, pH 8, 150 mM NaCl, 1.5 mM $MgCl_2$, 1% glycerol, 1% TritonX100, 0.5 mM EDTA, pH 8, and 5 mM NaF) supplemented with a protease inhibitor cocktail (11873580001; Sigma-Aldrich) and phosphatase inhibitor cocktail (78420; Thermo Fisher Scientific). Postnuclear lysates obtained by centrifugation at maximum velocity for 15 min at 4°C and were kept at −20°C before immunoblot analysis.

Preparation of LAT-containing membranes

To prepare membranes containing LAT, JCAM2.5 LAT-deficient Jurkat cells expressing the mouse LAT-TST protein (Roncagalli et al., 2014) were suspended in 0.25 M sucrose, 10 mM Tris-HCl, pH 7.4, and 1 mM EDTA (homogenization buffer) supplemented with a protease inhibitor cocktail (Sigma-Aldrich) and a phosphatase inhibitor cocktail (Thermo Fisher Scientific) and then transferred into a Dounce homogenizer (Kimble Kontes). Cell breakage was induced on ice by 25 successive stokes. The cell suspension was then passed 15 times through a 25-Ga needle to achieve cell disruption and centrifuged for 5 min at 900 *g* at 4°C to remove nuclei and intact cells. The supernatant was transferred into Ultra-clear centrifugation tubes (Beckman Coulter) and centrifuged at 65,000 *g* for 1 h at 4°C in a SW55Ti rotor (Beckman Coulter). The pellet was suspended in 1.2 ml of homogenization buffer supplemented as before and passed several times through a 25-Ga needle to ensure complete resuspension of the membranes. This suspension was transferred into a new tube and mixed with 1.2 ma of a 60% solution of Optiprep/iodixanol (Axis-Shield) to reach a 30% iodixanol suspension. The Optiprep solution was diluted extemporaneously into 0.25 M sucrose, 60 mM Tris-HCl, pH 7.4, and 6 mM EDTA to prepare 1.3 ml of a 20% solution and 1.2 ml of a 10% solution. The 20% and the 10% iodixanol solutions were layered successively on top of the 30% suspension and centrifuged at 350,000*g* for 3 h at 4°C in a SW55Ti rotor (342194; Beckman Coulter) without brake when stopping. Ten fractions of 490 µl were collected from the top of the tube. To purify LAT-*Strep*Tag–associated membranes, fraction 3 was incubated for 90 min at 4°C on a rotating wheel with equal amounts of either prewashed Sepharose resin (IBA GmbH) or prewashed *Strep*-Tactin Sepharose resin in the presence of protease and phosphatase inhibitors. Resins were washed and suspended in *Strep*Tag washing buffers (buffer W, 100 mM, Tris-HCl, 150 mM NaCl, and 1 mM, EDTA, pH 8.0) according to the manufacturer's instructions. After 5 washes in buffer W, membranes were eluted from the resin by incubation for 8 min at 4°C with 2.5 mM of D-biotin (Sigma-Aldrich) diluted in buffer W. Eluted material was then submitted to SDS-PAGE and immunoblot analysis.

SNAP-tag capture assay

Jurkat cells expressing both the GalT-GFP-SNAP and the HA-LAT encoding constructs were incubated for 30 min at 4°C on a wheel with 1:100 of mouse anti-HA Ab (901515; Biolegend). The cells were washed with cold PBS and incubated for 45 min at 4°C on a wheel with membrane-impermeable BG–PEG9–NHS (Johannes and Shafaq-Zadah, 2013). Cells were then incubated 4 h at 37°C in complete medium to analyze constitutive traffic of endocytosed LAT or put on slides together with Raji B cells for 30 min to form conjugates as described in the "Preparation of Jurkat T cells and Raji B cells conjugates" section. Cells were then fixed and permeabilized and stained with anti-GFP (human anti-GFP from Institut Curie) to reveal the GalT-GFP-SNAP and anti–mouse Ig to reveal the anti-HA Ab. Colocalization of the proteins was analyzed as described in the "Analysis of HA-LAT trapping in Golgi in cells expressing SNAP-Tag" section.

Immunoblot analysis

Protein concentrations from mouse samples were determined with microBCA kit (23235; Thermo Fisher Scientific) by diluting the samples to 1:50, and 10 µg of protein was loaded. NuPage LDS loading buffer (NP0008; Thermo Fisher Scientific) and reducing agent (NP0009; Thermo Fisher Scientific) were added to postnuclear lysates that were heated at 95°C for 5 min. Samples were resolved on NuPage 4–12% Bis-Tris gel (NP0323BOX; Thermo Fisher Scientific) and liquid

transferred (NP00061; Thermo Fisher Scientific) on PVDF membranes (162-0177; Biorad). After blocking with 1× TBS, 0.05% Tween20, 5% BSA for 1 h 30 min on a rocking platform shaker, membranes were incubated overnight at 4°C with primary antibodies anti-Rab6 (0.2 µg/ml, sc-310; Santa Cruz Biotechnology), anti–α-tubulin (1:1,000, CP08; Calbiochem), anti–phospho-LAT Y191 (1:1,000, 07-278; Millipore), anti–phospho-CD3ζ Y142 (1:1,000, 558402; BD Biosciences), anti–Syntaxin-16 (0.1 µg/ml, ab134945; Abcam) or anti-gp96 (1:1,000, ADI-SPA-850; Enzo), anti-LAMP1 (1:1,000, 3243; Cell Signaling Technology), anti-GM130 (1:1,000, ab52649; Abcam), and anti–Vps-35 (1:1,000, ab10099; Abcam). Membranes were washed three times with TBS 0.05% Tween and incubated for 40 min in TBS 0.05% Tween on rocking platform shaker with the following secondary antibodies (1:20,000; Jackson ImmunoResearch): anti–rabbit HRP (111-036-046), anti–mouse HRP (115-035-146), or anti–rat HRP (112-035-143) according to primary antibody species. Membranes were washed three times and incubated for 1 min with HRP substrate (Enhanced Chemiluminescence, 32106; Thermo Fisher Scientific). Autoradiography films (28906844; Amersham) were exposed to membranes for different exposure times and were revealed with an AGFA CP100 film processor.

Immunofluorescence

Coverslip and dish preparation. 12-mm-diameter coverslips (631-0666; VWR) were precoated with poly-L-lysine (0.02%, P8920; Sigma-Aldrich) for 20 min at room temperature and were washed three times in water before being dried and kept for a maximum of 2 d.

Preparation of Jurkat T cells and Raji B cells conjugates. Raji B cells were washed, resuspended at a concentration of 10^6 cells/ml in RPMI without FCS, and labeled with CellTracker Blue CMAC dye (10 µM, C2110; Thermo Fisher Scientific) for 20 min in a 37°C waterbath. Labeling was stopped with RPMI 10% FCS, and cells were washed once and resuspended at 10^6 cells/ml. Cells were pulsed with SEE (100 ng/ml) or left untreated for 30 min at 37°C in a water bath before being washed once and resuspended at a concentration of 0.5×10^6 cells/ml. 75,000 Raji cells were incubated on coverslips for 30 min and washed once with warmed PBS, and 150,000 Jurkat cells resuspended in RPMI 10% FCS were added for 30 min. Coverslips were washed once with cold PBS before fixation.

Fixed TIRFM. Poly-L-lysine–coated coverslips were left untreated or coated overnight at 4°C or 3–4 h at 37°C with αCD3εαCD28 (human or mouse–specific), washed three times, and prewarmed at 37°C for 10–15 min. 150,000 Jurkat T cells or mouse $CD4^+$ T cells were incubated on coated coverslips for 10 min before being washed once with cold PBS and fixed.

Fixation. Cells were fixed with 4% paraformaldehyde (15710; Electron Microscopy Sciences) for 15 min at room temperature and washed once in PBS, and excess paraformaldehyde was quenched for 10 min with PBS 10 mM Glycine (G8898; Thermo Fisher Scientific). Coverslips were kept at 4°C in PBS until permeabilization and staining.

Staining. For regular staining, cells were permeabilized for 30 min at room temperature with PBS 0.2% BSA (04–100-812; Euromedex) and 0.05% Saponin (S4521; Sigma-Aldrich). Cells were incubated for 1 h at room temperature with the following primary antibodies: rabbit anti-LAT (5 µg/ml, 06–807; Millipore), mouse anti-LAT (5 µg/ml, MAB63341; R&D Systems), rabbit anti–phospho-LAT (1:50, 3584; Cell Signaling Technology), rabbit anti–phospho-ZAP70 (1:50, 27015; Cell Signaling Technology), anti-ZAP70 (1:400, 3165; Cell Signaling Technology), rabbit anti-GFP (1:200, A11122; Thermo Fisher Scientific), mouse anti-GFP (1:200, A11120; Thermo Fisher Scientific) or human anti-GFP (produced by the Institut Curie platform), anti-Rab6 (1:400, 9625; Cell Signaling Technology), and anti–Syntaxin-16 (5 µg/ml, ab134945; Abcam) or anti-Giantin (produced by the Institut Curie platform). Cells were washed three times with 1× PBS, 0.2% BSA, 0.05% Saponin and incubated protected from light for 30 min in the same buffer with spinned secondary antibodies (1:300) anti–rabbit Ig Alexa Fluor 568 (A11036; Thermo Fisher Scientific), anti–rabbit Ig Alexa Fluor 488 (A11034; Thermo Fisher Scientific), anti–mouse Ig Alexa Fluor 568 (A11004; Thermo Fisher Scientific), anti–mouse Ig Alexa Fluor 488 (A11029; Thermo Fisher Scientific), or anti–human Ig Cy2 (709–225-149; Jackson Immunoresearch Laboratories) according to primary antibody species. After washing once with PBS BSA Saponin, and once with PBS, coverslips were soaked three times in PBS and three times in water and mounted on slides. For VAMP7 endogenous staining, cells were treated as in Larghi et al. (2013).

Mounting. For regular confocal microscopy, coverslips were mounted with 4–6 µl of Fluoromount G (0100–01; SouthernBiotech) on slides (KNITTEL Starfrost) and dried overnight protected from light before microscope acquisition.

For TIRFM, after staining with secondary antibody, coverslips were soaked in PBS and mounted with 4–6 µl of PBS, sealed with uncolored nail polish, and dried for 15 min before acquisition.

Microscopy and image analysis

Microscopes. Confocal images were acquired with a Laser Scanning Confocal (LSM780; Zeiss) from the PICT-IBiSA @ Pasteur Imaging Facility at Institut Curie, equipped with 40× or 100× Plan Apo objectives (numerical apertures, 1.35), and a 1–airy unit pinhole size was used. Single-plane images or z-stack images were acquired. TIRFM was performed using an inverted Nikon microscope Ti-E from the Nikon Imaging Center at Institut Curie-CNRS with a 100× CFI Apo TIRF and equipped with objective (numerical aperture of 1.49), 491 nm and 561 nm lasers, and an EMCCD 512 Evolve cam-

era (Photometrics). Images were analyzed on Fiji (Schindelin et al., 2012), and ImageJ software and compatible scripts were generated for automated or semiautomated analysis.

Analysis of LAT recruitment to the immune synapse between Jurkat and Raji conjugates on confocal images and "mean cell" creation. Middle plane images with from similarly dimensioned z-stack images of conjugates were chosen, and T cells were cropped and oriented in the same way regarding their synapse (script 1). Created images were grouped by condition (shRNA ± SEE), and fluorescence intensities were normalized by the mean fluorescence intensity (MFI) of all images. Images were then resized to the smallest image size in order to create stacks of images for each group (script 2). Each stack was normalized to MFI, mean height, and mean width of all groups in order to obtain conditions with comparable total cell MFI and identical sizes. Stacks of aligned cells were finally projected (averaging method), giving single-plane "mean cells" (script 3). Then, in order to obtain mean intensity profiles along cell width, stacks of images from script 2 were normalized to MFI and mean width of all experimental groups and were resized to obtain a 1-pixel height stack by averaging the fluorescence intensity of the total height of each image. Projected images were created based on mean and SD methods, and pixel intensities were measured along image widths (script 4). To get a cell-by-cell quantification, MFI of total cells and MFI of rectangles at the synapse region representing 10.5% of the total cells were measured plane by plane for each stack from script 2. Ratios of both MFIs were calculated, giving LAT enrichment at the immune synapse, expressed in arbitrary units (script 3).

Analysis of the recruitment of molecules to the immune synapse on TIRFM images. Before imaging cells, TIRFM angle was set up to provide an evanescent field of fixed thickness (~120–150 nm). Illuminated microclusters were imaged, and the background was substracted (50 pixels, rolling ball radius) for each acquired image. Cells were manually segmented, and regions of interest (ROIs) were defined in order to measure their areas. Then, within each ROI, microclusters present in the evanescent field were defined as signal intensity maxima detected by using the "Find Maxima…" method, for which a value of noise tolerance was arbitrarily set according to background from experiment to experiment (values around 5,000 in most experiments). Using this method allowed the discrimination of maximas coming from clusters (local bright patches at the plasma membrane or just below in the limit of thickness of the evanescent field) from an homogeneous signal. The number of "maximas" was then counted for each ROI, giving a cell-by-cell quantification of the number of microclusters or density of microclusters at or below the plasma membrane.

Analysis of colocalization on confocal images based on overlapped areas. Middle planes of z-stack images of similarly dimensioned conjugates were chosen. Masks for Raji B cells labeled with CellTracker Blue CMAC dye were obtained by automatic thresholding ("Otsu" method). Masks of T-B conjugates were created with LAT staining background by using automatic thresholding ("Default" method). B masks were substracted from T-B masks, creating T masks that were defined as ROIs by using the "Analyze Particles…" function. Within each ROI, a Golgi mask based on Rab6 or Syntaxin-16 staining was created by thresholding. LAT areas, Golgi areas, and overlapping areas were calculated, and ratios of overlapping areas/LAT areas were calculated and expressed in arbitrary units.

Analysis of HA-LAT trapping in Golgi in cells expressing SNAP-Tag. Z-stack (0.5 µm) images of similarly dimensioned conjugates or Jurkat cells were chosen. In that z-stack, a ROI surrounding the Golgi was defined based on GalT-GFP-SNAP staining. Within each ROI, masks based on both GalT-GFP-SNAP and HA-LAT stainings were created by thresholding. Automatic colocalization assays were performed with Mander's overlap coefficient, using the JACoP plugin for ImageJ64. Colocalization plots, in representative images showing the maximum intensity from z-projections of three to five z-stacks, were obtained using the "RGB Profiler" plugins on ImageJ.

IL-2 secretion and production assay in Jurkat cells. Jurkat T cells and Raji B cells were washed and resuspended at 10^6 cells/ml. 100 µl Jurkat cells and 50 µl Raji cells were mixed in a 96-well plate, flat bottom (92096; TPP). 50 µl of SEE at the final indicated concentrations was added for 6 h. Supernatants were recovered and tested for IL-2 by ELISA (BD OptEIA, 555190; BD Biosciences). Total mRNA was isolated from cells with NucleoSpin RNA kit (740–955; Macherey Nagel), and IL-2 mRNA expression was assessed by quantitative PCR using the Taqman method and IL-2 mRNA targeting primers (Hs00174114_m1; Thermo Fisher Scientific). For intracellular cytometry, after 1 h activation, 25 µl of brefeldin-A (B6542; Sigma-Aldrich), at the final concentration of 5 µg/ml, was added to each well for an additional 5 h.

Mixed lymphocyte reaction

Spleens from BalB/C mice were dissociated into cell suspension, filtered, irradiated (20 Gy), and used as stimulatory cells. In the case of separated culture of Rab6 cKO and control $CD4^+$ T cells, stimulatory cells and responder cells were respectively labeled with CFSE dye (2 µM, C34554; Thermo Fisher Scientific) and CellTrace Violet (CTV) dye (2 µM, C34557; Thermo Fisher Scientific). 4×10^5 responder cells were cocultured with indicated numbers of stimulatory cells. In the case of Rab6 cKO and control responder cells coculture, control and cKO cells were respectively stained with CTV and CFSE dyes and mixed with the indicated amount of stimulatory cells. As positive control, cell proliferation was induced with phorbol myristate acetate (7.5×10^{-7} M) and ionomycin (2×10^{-8} M).

Cells were cocultured for 5 d at 37°C, 5% CO_2, in complete medium before being stained for flow cytometry analysis.

BM chimeras and immunizations

Reconstitution. Rag2 KO mice were irradiated (5.5 Gy) and reconstituted with filtered BM cells from control or Rab6 cKO mice. After 8–10 wk of reconstitution, mice were bled, and reconstitution was assessed by flow cytometry.

Immunization. BM chimeras were subcutaneously injected at the right flank with 100 µg OVA (A5503; Sigma-Aldrich) or 100 µg OVA emulsified with CFA (11719062; Fisher Scientific). After 11 d of immunization, mice were sacrificed, and spleen and draining inguinal LN were harvested and dissociated into single-cell suspensions. Suspension was then filtered and red blood cells lysed (R7757; Sigma-Aldrich) before cell counting with a MACS Quant flow cytometer. 10^6, 0.5×10^6, and 0.2×10^6 cells/well were seeded in nonactivated ELI SPOT plates (MAIPS4510; Millipore), precoated overnight at 4°C with anti–IFN-γ (2 µg/ml, clone AN-18, 14–7313; eBioscience), anti–IL-17A (88–7370-88; eBioscience), anti–IL-2 (5 µg/ml, clone JES6-1A12, 14–7022; eBioscience), anti–IL-4 (2 µg/ml, clone 11B11, 14–7041; eBioscience), or anti–IL-5 (2 µg/ml, clone TRFK5, 14–7052; eBioscience) capture antibodies diluted in ELISPOT coating buffer (16–000-27; eBioscience) and washed three times with complete medium. Cells were restimulated with irrelevant antigen (50 µg/ml HSA, SRP6182; Sigma-Aldrich), OVA protein used for immunization (50 µg/ml), MHC class I peptide ($OVA_{257-264}$, 10 µg/ml, vac-sin; Invivogen), MHC class II peptide ($OVA_{323-339}$, 10 µg/ml, vac-isq; Invivogen), and phorbol myristate acetate (7.5×10^{-7} M) and ionomycin (2×10^{-8} M). IFN-γ, IL-17A, and IL-2 responses were assessed 24 h after stimulation, whereas IL-4 and IL-5 secretions were analyzed 48 h after restimulation. ELISPOT plates were washed three times with PBS 0.05% Tween and incubated overnight at 4°C with biotinylated detection antibodies, anti–IFN-γ (2 µg/ml, clone R4-6A2, 13-7312; eBioscience), anti–IL-17A (88-7370-88; eBioscience), anti–IL-2 (5 µg/ml, clone JES6-5H4, 13-7021; eBioscience), anti–IL-4 (1 µg/ml, clone BVD6-24G2, 13-7042; eBioscience), and anti–IL-5 (1 µg/ml, clone TRFK4, 13-7051; eBioscience) diluted in ELISPOT buffer (00-4202-55; eBioscience). Plates were washed four times with PBS 0.05% Tween and incubated with streptavidin-conjugated alkaline phosphatase (1:1,000, 3310-10; MABtech) diluted in ELISPOT buffer. After 45 min incubation at room temperature, plates were washed three times in PBS 0.05% and twice with PBS before adding alkaline phosphatase substrate (170-6432; Biorad). The reaction was stopped with water, and plates were dried out before spot-counting with an AID EliSpot reader.

Flow cytometry

In all conditions, cells were centrifuged and transferred to a conical-bottom plate (650101; Greiner Bio-One), stained in PBS with Fixable Viability Dye eFluor 780 (1:4,000, 65-0865-18; eBioscience), and washed in FACS Buffer (1× PBS, 0.5% BSA, 2 mM EDTA). Extracellular staining was performed in FACS Buffer for 30 min on ice. For surface marker expression of human cells, anti-TCRα/β PE (1:20, A39499; Beckman Coulter), anti-CD3ε Alexa Fluor 647 (1:100, 557706; BD PharMingen), anti-CD28 PE (1:100, 555729; BD PharMingen), and mouse anti-HA (901515; Biolegend) were used. For IL-2 detection, anti–human CD19 PE-Cy7 (1:100, 25-0198; eBioscience) was used to exclude Raji B cells from analysis.

For mouse sample staining, cells were stained on ice for 30 min with 50 µl of FcBlock diluted in FACS buffer (1:25, 553142; BD PharMingen). For mixed lymphocyte reaction analysis, 50 µl of anti-CD4 APC (1:150, 553051; BD PharMingen) and anti–MHC-II APC-eFluor 780 (1:250, 47-5321-82; eBioscience) were directly added 30 min before fixation. Proliferating cells were gated on live MHC-II$^-$ CFSE$^-$ cells (to exclude the stimulatory BalbC cells) and CD4$^+$ cells. For immune compartments phenotyping, different antibody mixes were used (1:300 final): anti-B220 FITC (553087; BD PharMingen), anti-CD3ε APC (553066; BD PharMingen), anti-CD4 PerCP (553052; BD PharMingen), anti-CD8α Pacific Blue (558106; BD PharMingen), anti-CD62L PE-Cy7 (560516; BD PharMingen), anti-CD44 PE (553134; BD PharMingen), anti-B220 APC (553092; BD PharMingen), anti–TCRβ-FITC (553171; BD PharMingen), anti-CD4 Pacific Blue (558107; BD PharMingen), anti-CD8α PE-Cy7 (552877; BD PharMingen), anti-CD25 PerCP-Cy5.5 (553077; BD PharMingen), anti-B220 eFluor 450 (48-0452-82; eBioscience), anti-CD25 FITC (553077; BD PharMingen), anti-CD11c PE Cy7 (558079; BD PharMingen), anti-I-Ab FITC (553551; BD PharMingen), anti-CD11b PerCP-Cy5.5 (550993; BD PharMingen), anti-CD11c APC (550261; BD PharMingen), anti–CD28-biotinylated (1:100, 553296; BD PharMingen), and streptavidin-PE (1:300, 554061; BD PharMingen).

Cells were washed in FACS Buffer and fixed with Cytofix/Cytoperm (554714; BD Biosciences) for regular cytometry or Fixation/Permeabilization buffer (00–5123-43 and 00–5223-56; eBioscience) for FoxP3 staining. For intracellular cytometry, cells were washed twice in Perm/Wash buffer (554723; BD Biosciences) for regular intracellular cytometry and Perm buffer (00–8333-56; eBioscience) for FoxP3 staining and intracellularly stained in respective buffer with anti–human IL-2 PE (1:50, 01-12-7029; eBioscience), anti-LAT (5 µg/ml, MAB63341; R&D Systems), anti–mouse PE (1:300, 115-116-146; Jackson ImmunoResearch) and anti–mouse FoxP3 (1:100, 12–5773-82; eBioscience).

For blood samples, 50 µl of blood was stained for 30 min, fixed with Lysing Buffer (349202; BD Biosciences), and washed several times before acquisition.

Cells and compensation beads (01–1111-42; eBioscience) were acquired with BD FACS Verse and MACS Quant (Miltenyi) flow cytometer, and data were analyzed with FlowJo software.

Statistical analysis

Statistical analysis was performed with GraphPad Prism 7 software. Data were considered statistically significant if the p-value obtained was lower than 0.05. Data were compared with the unpaired Student's *t* tests for values following a Gaussian distribution with similar variances. For multigroup comparisons, we applied one-way or two-way ANOVA.

Online supplemental material

Fig. S1 shows defect in LAT recruitment at the IS in Jurkat T cells silenced for VAMP7. Fig. S2 shows the principle of the SNAP-tag capture assay and several controls for this method. It also shows the absence of retrograde LAT trafficking to the IS after 30 min in the absence of TCR triggering. Fig. S3 shows the decreased expression of Rab6 and Syntaxin-16 in Jurkat cells expressing the corresponding shRNA. It also shows that CD3, CD28, and total LAT expression are not affected in silenced cells, whereas at steady-state LAT presence at the plasma membrane is increased. Fig. S4 characterizes the immune compartments in Rab6 cKO mice. It shows that percentages of the different thymic T cell populations are normal, as well as T and B cell percentages in LN, mLN, and BM; regulatory T cell percentages in spleen and thymus; and percentages and numbers of DC populations, macrophages, and neutrophils. Data show that CD4, CD3ε, and CD28 expression as well as total LAT expression are normal in $CD4^+$ T lymphocytes from Rab6 cKO mice. Fig. S5 shows that chimeras reconstituted with bone marrow from Rab6 cKO mice present normal percentages of T cells and B cells 8 to 10 wk after reconstitution but that immunization of the mice with CFA/OVA induces less IL-2, IL-5, and IL-4 production by T cells as revealed by ELISPOT of the chimera splenocytes restimulated in vivo with OVA or OVA peptides.

ACKNOWLEDGMENTS

We thank C. Daviaud, O. Lebhar, P. Parent, and J. Sempe and all the staff from the animal facility, Institut Curie, Paris, France; P. Le Baccon from the PICT-IBiSA@Pasteur microscopy facility, Institut Curie, Paris, France; the PICT-IBiSA, member of the France-BioImaging national research infrastructure, supported by the French National Research Agency (ANR) through the "Investments for the Future" program (ANR-10-INSB-04) and the CelTisPhyBio Labex (ANR-10-LBX-0038), part of the IDEX PSL (ANR-10-IDEX-0001-02 PSL); L. Sengmanivong and all the staff from the Nikon Imaging Center (Institut Curie, Centre National de la Recherche Scientifique, Paris, France); F.-X. Gobert for P3 training and coordination (Institut Curie, Institut National de la Santé et de la Recherche Medicale U932, Paris, France); S. Heinrich for x-ray generator training and dosimetry (Institut Curie, Paris, France); S. Moutel from Antibody Platform (Institut Curie, Paris, France); and B. Malissen and R. Roncagalli (CIML, Marseille, France) for giving us the LAT-TST constructs.

J.-M. Carpier received grants from La Ligue Nationale Contre le Cancer and Fondation pour la Recherche Médicale (FDT20150532086), and A.E. Zucchetti from l'Association pour la Recherche sur le Cancer. Work was supported by funds from Institut Curie, Institut National de la Santé et de la Recherche Médicale, ANR (ANR-13-BSV2-0018 "NeuroImmunoSynapse," ANR-10-IDEX-0001-02 PSL*, and ANR-11-LABX-0043), the Fondation pour la Recherche Médicale (FRM DEQ20140329513), European Research Council advanced grants to B. Goud (339847 "MYO DYN") and L. Johannes (340485 "GalectCompart"), and the European Union's Horizon 2020 research and innovation programme under the Marie Skłodowska-Curie grant agreement no. 675007.

The authors declare no competing financial interests.

Author contributions: J.-M. Carpier designed, performed, and analyzed most of the microscopy experiments (except capture assay, Fig. 3), all functional experiments on silenced Jurkat T cells, and all in vivo and ex vivo analysis of mouse T lymphocytes, and prepared and contributed to writing the manuscript. A.E. Zucchetti set up, performed, and analyzed experiments in Fig. 3 and Fig. S2; performed and analyzed some microscopy experiments from Figs. 1 and 4; and contributed to writing the manuscript. L. Bataille performed experiments shown in Fig. 2 and Fig. 4 (D and E). S. Dogniaux prepared shRNA lentivirus and purified plasmids encoding chimeric molecules, performed qPCR analysis and some ELISAs from Fig. 5, and genotyped mice. M. Shafaq-Zadah performed and analyzed experiments from Fig. 3 and Fig. S2 together with A.E. Zucchetti. S. Bardin purified plasmids and provided key material, i.e., antibodies. M. Lucchino prepared BG-PEG9-NHS. M. Maurin analyzed microscopy experiments. L.D. Joannas performed some mouse experiments together with J.-M. Carpier. J.G. Magalhaes performed some mouse experiments together with J.-M. Carpier. L. Johannes helped to design experiments on retrograde transport. T. Galli helped to design experiments and discussed the results. B. Goud designed $Rab6^{fl/fl}$ mice and discussed the results. C. Hivroz conceived the study and wrote the manuscript.

Submitted: 20 December 2016

Revised: 30 November 2017

Accepted: 11 January 2018

REFERENCES

Amessou, M., A. Fradagrada, T. Falguières, J.M. Lord, D.C. Smith, L.M. Roberts, C. Lamaze, and L. Johannes. 2007. Syntaxin 16 and syntaxin 5 are required for efficient retrograde transport of several exogenous and endogenous cargo proteins. *J. Cell Sci.* 120:1457–1468. https://doi.org/10.1242/jcs.03436

Antón, O.M., L. Andrés-Delgado, N. Reglero-Real, A. Batista, and M.A. Alonso. 2011. MAL protein controls protein sorting at the supramolecular activation cluster of human T lymphocytes. *J. Immunol.* 186:6345–6356. https://doi.org/10.4049/jimmunol.1003771

Arighi, C.N., L.M. Hartnell, R.C. Aguilar, C.R. Haft, and J.S. Bonifacino. 2004. Role of the mammalian retromer in sorting of the cation-independent mannose 6-phosphate receptor. *J. Cell Biol.* 165:123–133. https://doi.org/10.1083/jcb.200312055

Balagopalan, L., V.A. Barr, C.L. Sommers, M. Barda-Saad, A. Goyal, M.S. Isakowitz, and L.E. Samelson. 2007. c-Cbl-mediated regulation of LAT-nucleated signaling complexes. *Mol. Cell. Biol.* 27:8622–8636. https://doi.org/10.1128/MCB.00467-07

Balagopalan, L., B.A. Ashwell, K.M. Bernot, I.O. Akpan, N. Quasba, V.A. Barr, and L.E. Samelson. 2011. Enhanced T-cell signaling in cells bearing linker for activation of T-cell (LAT) molecules resistant to ubiquitylation. *Proc. Natl. Acad. Sci. USA.* 108:2885–2890. https://doi.org/10.1073/pnas.1007098108

Balagopalan, L., V.A. Barr, R.L. Kortum, A.K. Park, and L.E. Samelson. 2013. Cutting edge: cell surface linker for activation of T cells is recruited to microclusters and is active in signaling. *J. Immunol.* 190:3849–3853. https://doi.org/10.4049/jimmunol.1202760

Bardin, S., S. Miserey-Lenkei, I. Hurbain, D. Garcia-Castillo, G. Raposo, and B. Goud. 2015. Phenotypic characterisation of RAB6A knockout mouse embryonic fibroblasts. *Biol. Cell.* 107:427–439. https://doi.org/10.1111/boc.201400083

Barr, V.A., L. Balagopalan, M. Barda-Saad, R. Polishchuk, H. Boukari, S.C. Bunnell, K.M. Bernot, Y. Toda, R. Nossal, and L.E. Samelson. 2006. T-cell antigen receptor-induced signaling complexes: internalization via a cholesterol-dependent endocytic pathway. *Traffic.* 7:1143–1162. https://doi.org/10.1111/j.1600-0854.2006.00464.x

Bivona, T.G., I. Pérez De Castro, I.M. Ahearn, T.M. Grana, V.K. Chiu, P.J. Lockyer, P.J. Cullen, A. Pellicer, A.D. Cox, and M.R. Philips. 2003. Phospholipase Cgamma activates Ras on the Golgi apparatus by means of RasGRP1. *Nature.* 424:694–698. https://doi.org/10.1038/nature01806

Blanchard, N., V. Di Bartolo, and C. Hivroz. 2002. In the immune synapse, ZAP-70 controls T cell polarization and recruitment of signaling proteins but not formation of the synaptic pattern. *Immunity.* 17:389–399. https://doi.org/10.1016/S1074-7613(02)00421-1

Bonello, G., N. Blanchard, M.C. Montoya, E. Aguado, C. Langlet, H.T. He, S. Nunez-Cruz, M. Malissen, F. Sanchez-Madrid, D. Olive, et al. 2004. Dynamic recruitment of the adaptor protein LAT: LAT exists in two distinct intracellular pools and controls its own recruitment. *J. Cell Sci.* 117:1009–1016. https://doi.org/10.1242/jcs.00968

Bonifacino, J.S., and R. Rojas. 2006. Retrograde transport from endosomes to the trans-Golgi network. *Nat. Rev. Mol. Cell Biol.* 7:568–579. https://doi.org/10.1038/nrm1985

Bouchet, J., I. Del Río-Iñiguez, R. Lasserre, S. Agüera-Gonzalez, C. Cuche, A. Danckaert, M.W. McCaffrey, V. Di Bartolo, and A. Alcover. 2016. Rac1-Rab11-FIP3 regulatory hub coordinates vesicle traffic with actin remodeling and T-cell activation. *EMBO J.* 35:1160–1174. https://doi.org/10.15252/embj.201593274

Brignatz, C., A. Restouin, G. Bonello, D. Olive, and Y. Collette. 2005. Evidences for ubiquitination and intracellular trafficking of LAT, the linker of activated T cells. *Biochim. Biophys. Acta.* 1746:108–115. https://doi.org/10.1016/j.bbamcr.2005.08.009

Burgo, A., V. Proux-Gillardeaux, E. Sotirakis, P. Bun, A. Casano, A. Verraes, R.K. Liem, E. Formstecher, M. Coppey-Moisan, and T. Galli. 2012. A molecular network for the transport of the TI-VAMP/VAMP7 vesicles from cell center to periphery. *Dev. Cell.* 23:166–180. https://doi.org/10.1016/j.devcel.2012.04.019

Chaineau, M., L. Danglot, and T. Galli. 2009. Multiple roles of the vesicular-SNARE TI-VAMP in post-Golgi and endosomal trafficking. *FEBS Lett.* 583:3817–3826. https://doi.org/10.1016/j.febslet.2009.10.026

Chemin, K., A. Bohineust, S. Dogniaux, M. Tourret, S. Guégan, F. Miro, and C. Hivroz. 2012. Cytokine secretion by CD4+ T cells at the immunological synapse requires Cdc42-dependent local actin remodeling but not microtubule organizing center polarity. *J. Immunol.* 189:2159–2168. https://doi.org/10.4049/jimmunol.1200156

Daniels, M.A., E. Teixeiro, J. Gill, B. Hausmann, D. Roubaty, K. Holmberg, G. Werlen, G.A. Holländer, N.R. Gascoigne, and E. Palmer. 2006. Thymic selection threshold defined by compartmentalization of Ras/MAPK signalling. *Nature.* 444:724–729. https://doi.org/10.1038/nature05269

Das, V., B. Nal, A. Dujeancourt, M.I. Thoulouze, T. Galli, P. Roux, A. Dautry-Varsat, and A. Alcover. 2004. Activation-induced polarized recycling targets T cell antigen receptors to the immunological synapse; involvement of SNARE complexes. *Immunity.* 20:577–588. https://doi.org/10.1016/S1074-7613(04)00106-2

Ehrlich, L.I., P.J. Ebert, M.F. Krummel, A. Weiss, and M.M. Davis. 2002. Dynamics of p56lck translocation to the T cell immunological synapse following agonist and antagonist stimulation. *Immunity.* 17:809–822. https://doi.org/10.1016/S1074-7613(02)00481-8

Finco, T.S., T. Kadlecek, W. Zhang, L.E. Samelson, and A. Weiss. 1998. LAT is required for TCR-mediated activation of PLCgamma1 and the Ras pathway. *Immunity.* 9:617–626. https://doi.org/10.1016/S1074-7613(00)80659-7

Finetti, F., S.R. Paccani, M.G. Riparbelli, E. Giacomello, G. Perinetti, G.J. Pazour, J.L. Rosenbaum, and C.T. Baldari. 2009. Intraflagellar transport is required for polarized recycling of the TCR/CD3 complex to the immune synapse. *Nat. Cell Biol.* 11:1332–1339. https://doi.org/10.1038/ncb1977

Finetti, F., L. Patrussi, G. Masi, A. Onnis, D. Galgano, O.M. Lucherini, G.J. Pazour, and C.T. Baldari. 2014. Specific recycling receptors are targeted to the immune synapse by the intraflagellar transport system. *J. Cell Sci.* 127:1924–1937. https://doi.org/10.1242/jcs.139337

Follit, J.A., R.A. Tuft, K.E. Fogarty, and G.J. Pazour. 2006. The intraflagellar transport protein IFT20 is associated with the Golgi complex and is required for cilia assembly. *Mol. Biol. Cell.* 17:3781–3792. https://doi.org/10.1091/mbc.E06-02-0133

Follit, J.A., J.T. San Agustin, F. Xu, J.A. Jonassen, R. Samtani, C.W. Lo, and G.J. Pazour. 2008. The Golgin GMAP210/TRIP11 anchors IFT20 to the Golgi complex. *PLoS Genet.* 4:e1000315. https://doi.org/10.1371/journal.pgen.1000315

Fooksman, D.R., S. Vardhana, G. Vasiliver-Shamis, J. Liese, D.A. Blair, J. Waite, C. Sacristán, G.D. Victora, A. Zanin-Zhorov, and M.L. Dustin. 2010. Functional anatomy of T cell activation and synapse formation. *Annu. Rev. Immunol.* 28:79–105. https://doi.org/10.1146/annurev-immunol-030409-101308

Goud, B., A. Zahraoui, A. Tavitian, and J. Saraste. 1990. Small GTP-binding protein associated with Golgi cisternae. *Nature.* 345:553–556. https://doi.org/10.1038/345553a0

Grakoui, A., S.K. Bromley, C. Sumen, M.M. Davis, A.S. Shaw, P.M. Allen, and M.L. Dustin. 1999. The immunological synapse: a molecular machine controlling T cell activation. *Science.* 285:221–227. https://doi.org/10.1126/science.285.5425.221

Hivroz, C., P. Larghi, M. Jouve, and L. Ardouin. 2017. Purification of LAT-Containing Membranes from Resting and Activated T Lymphocytes. *Methods Mol. Biol.* 1584:355–368. https://doi.org/10.1007/978-1-4939-6881-7_21

Hundt, M., Y. Harada, L. De Giorgio, N. Tanimura, W. Zhang, and A. Altman. 2009. Palmitoylation-dependent plasma membrane transport but lipid raft-independent signaling by linker for activation of T cells. *J. Immunol.* 183:1685–1694. https://doi.org/10.4049/jimmunol.0803921

Johannes, L., and V. Popoff. 2008. Tracing the retrograde route in protein trafficking. *Cell.* 135:1175–1187. https://doi.org/10.1016/j.cell.2008.12.009

Johannes, L., and M. Shafaq-Zadah. 2013. SNAP-tagging the retrograde route. *Methods Cell Biol.* 118:139–155. https://doi.org/10.1016/B978-0-12-417164-0.00009-4

Kupfer, A., G. Dennert, and S.J. Singer. 1983. Polarization of the Golgi apparatus and the microtubule-organizing center within cloned natural killer cells bound to their targets. *Proc. Natl. Acad. Sci. USA.* 80:7224–7228. https://doi.org/10.1073/pnas.80.23.7224

Larghi, P., D.J. Williamson, J.M. Carpier, S. Dogniaux, K. Chemin, A. Bohineust, L. Danglot, K. Gaus, T. Galli, and C. Hivroz. 2013. VAMP7 controls T cell activation by regulating the recruitment and phosphorylation of vesicular Lat at TCR-activation sites. *Nat. Immunol.* 14:723–731. https://doi.org/10.1038/ni.2609

Lillemeier, B.F., M.A. Mörtelmaier, M.B. Forstner, J.B. Huppa, J.T. Groves, and M.M. Davis. 2010. TCR and Lat are expressed on separate protein islands on T cell membranes and concatenate during activation. *Nat. Immunol.* 11:90–96. https://doi.org/10.1038/ni.1832

Lu, L., and W. Hong. 2014. From endosomes to the trans-Golgi network. *Semin. Cell Dev. Biol.* 31:30–39. https://doi.org/10.1016/j.semcdb.2014.04.024

Mallard, F., C. Antony, D. Tenza, J. Salamero, B. Goud, and L. Johannes. 1998. Direct pathway from early/recycling endosomes to the Golgi apparatus revealed through the study of shiga toxin B-fragment transport. *J. Cell Biol.* 143:973–990. https://doi.org/10.1083/jcb.143.4.973

Mallard, F., B.L. Tang, T. Galli, D. Tenza, A. Saint-Pol, X. Yue, C. Antony, W. Hong, B. Goud, and L. Johannes. 2002. Early/recycling endosomes-to-TGN transport involves two SNARE complexes and a Rab6 isoform. *J. Cell Biol.* 156:653–664. https://doi.org/10.1083/jcb.200110081

Martinez, O., A. Schmidt, J. Salaméro, B. Hoflack, M. Roa, and B. Goud. 1994. The small GTP-binding protein rab6 functions in intra-Golgi transport. *J. Cell Biol.* 127:1575–1588. https://doi.org/10.1083/jcb.127.6.1575

Martinez-Arca, S., P. Alberts, A. Zahraoui, D. Louvard, and T. Galli. 2000. Role of tetanus neurotoxin insensitive vesicle-associated membrane protein

(TI-VAMP) in vesicular transport mediating neurite outgrowth. *J. Cell Biol.* 149:889–900. https://doi.org/10.1083/jcb.149.4.889

Mayinger, P. 2011. Signaling at the Golgi. *Cold Spring Harb. Perspect. Biol.* 3:a005314. https://doi.org/10.1101/cshperspect.a005314

Onnis, A., F. Finetti, and C.T. Baldari. 2016. Vesicular Trafficking to the Immune Synapse: How to Assemble Receptor-Tailored Pathways from a Basic Building Set. *Front. Immunol.* 7:50. https://doi.org/10.3389/fimmu.2016.00050

Pocha, S.M., T. Wassmer, C. Niehage, B. Hoflack, and E. Knust. 2011. Retromer controls epithelial cell polarity by trafficking the apical determinant Crumbs. *Curr. Biol.* 21:1111–1117. https://doi.org/10.1016/j.cub.2011.05.007

Purbhoo, M.A. 2013. The function of sub-synaptic vesicles during T-cell activation. *Immunol. Rev.* 251:36–48. https://doi.org/10.1111/imr.12012

Purbhoo, M.A., H. Liu, S. Oddos, D.M. Owen, M.A. Neil, S.V. Pageon, P.M. French, C.E. Rudd, and D.M. Davis. 2010. Dynamics of subsynaptic vesicles and surface microclusters at the immunological synapse. *Sci. Signal.* 3:ra36. https://doi.org/10.1126/scisignal.2000645

Roncagalli, R., S. Hauri, F. Fiore, Y. Liang, Z. Chen, A. Sansoni, K. Kanduri, R. Joly, A. Malzac, H. Lähdesmäki, et al. 2014. Quantitative proteomics analysis of signalosome dynamics in primary T cells identifies the surface receptor CD6 as a Lat adaptor-independent TCR signaling hub. *Nat. Immunol.* 15:384–392. https://doi.org/10.1038/ni.2843

Samelson, L.E. 2002. Signal transduction mediated by the T cell antigen receptor: the role of adapter proteins. *Annu. Rev. Immunol.* 20:371–394. https://doi.org/10.1146/annurev.immunol.20.092601.111357

Schindelin, J., I. Arganda-Carreras, E. Frise, V. Kaynig, M. Longair, T. Pietzsch, S. Preibisch, C. Rueden, S. Saalfeld, B. Schmid, et al. 2012. Fiji: an open-source platform for biological-image analysis. *Nat. Methods.* 9:676–682. https://doi.org/10.1038/nmeth.2019

Seaman, M.N. 2004. Cargo-selective endosomal sorting for retrieval to the Golgi requires retromer. *J. Cell Biol.* 165:111–122. https://doi.org/10.1083/jcb.200312034

Seaman, M.N., J.M. McCaffery, and S.D. Emr. 1998. A membrane coat complex essential for endosome-to-Golgi retrograde transport in yeast. *J. Cell Biol.* 142:665–681. https://doi.org/10.1083/jcb.142.3.665

Shafaq-Zadah, M., C.S. Gomes-Santos, S. Bardin, P. Maiuri, M. Maurin, J. Iranzo, A. Gautreau, C. Lamaze, P. Caswell, B. Goud, and L. Johannes. 2016. Persistent cell migration and adhesion rely on retrograde transport of β(1) integrin. *Nat. Cell Biol.* 18:54–64. https://doi.org/10.1038/ncb3287

Sherman, E., V. Barr, S. Manley, G. Patterson, L. Balagopalan, I. Akpan, C.K. Regan, R.K. Merrill, C.L. Sommers, J. Lippincott-Schwartz, and L.E. Samelson. 2011. Functional nanoscale organization of signaling molecules downstream of the T cell antigen receptor. *Immunity.* 35:705–720. https://doi.org/10.1016/j.immuni.2011.10.004

Sherman, E., V.A. Barr, R.K. Merrill, C.K. Regan, C.L. Sommers, and L.E. Samelson. 2016. Hierarchical nanostructure and synergy of multimolecular signalling complexes. *Nat. Commun.* 7:12161. https://doi.org/10.1038/ncomms12161

Simonsen, A., B. Bremnes, E. Rønning, R. Aasland, and H. Stenmark. 1998. Syntaxin-16, a putative Golgi t-SNARE. *Eur. J. Cell Biol.* 75:223–231. https://doi.org/10.1016/S0171-9335(98)80116-7

Soares, H., R. Henriques, M. Sachse, L. Ventimiglia, M.A. Alonso, C. Zimmer, M.I. Thoulouze, and A. Alcover. 2013. Regulated vesicle fusion generates signaling nanoterritories that control T cell activation at the immunological synapse. *J. Exp. Med.* 210:2415–2433. https://doi.org/10.1084/jem.20130150

Stinchcombe, J.C., E. Majorovits, G. Bossi, S. Fuller, and G.M. Griffiths. 2006. Centrosome polarization delivers secretory granules to the immunological synapse. *Nature.* 443:462–465. https://doi.org/10.1038/nature05071

Su, X., J.A. Ditlev, E. Hui, W. Xing, S. Banjade, J. Okrut, D.S. King, J. Taunton, M.K. Rosen, and R.D. Vale. 2016. Phase separation of signaling molecules promotes T cell receptor signal transduction. *Science.* 352:595–599. https://doi.org/10.1126/science.aad9964

Tang, B.L., D.Y. Low, S.S. Lee, A.E. Tan, and W. Hong. 1998. Molecular cloning and localization of human syntaxin 16, a member of the syntaxin family of SNARE proteins. *Biochem. Biophys. Res. Commun.* 242:673–679. https://doi.org/10.1006/bbrc.1997.8029

Vivar, O.I., G. Masi, J.M. Carpier, J.G. Magalhaes, D. Galgano, G.J. Pazour, S. Amigorena, C. Hivroz, and C.T. Baldari. 2016. IFT20 controls LAT recruitment to the immune synapse and T-cell activation in vivo. *Proc. Natl. Acad. Sci. USA.* 113:386–391. https://doi.org/10.1073/pnas.1513601113

Weiss, A., and D.R. Littman. 1994. Signal transduction by lymphocyte antigen receptors. *Cell.* 76:263–274. https://doi.org/10.1016/0092-8674(94)90334-4

Williamson, D.J., D.M. Owen, J. Rossy, A. Magenau, M. Wehrmann, J.J. Gooding, and K. Gaus. 2011. Pre-existing clusters of the adaptor Lat do not participate in early T cell signaling events. *Nat. Immunol.* 12:655–662. https://doi.org/10.1038/ni.2049

Xie, J.J., J.Q. Liang, L.H. Diao, A. Altman, and Y. Li. 2013. TNFR-associated factor 6 regulates TCR signaling via interaction with and modification of LAT adapter. *J. Immunol.* 190:4027–4036. https://doi.org/10.4049/jimmunol.1202742

Yudushkin, I.A., and R.D. Vale. 2010. Imaging T-cell receptor activation reveals accumulation of tyrosine-phosphorylated CD3ζ in the endosomal compartment. *Proc. Natl. Acad. Sci. USA.* 107:22128–22133. https://doi.org/10.1073/pnas.1016388108

Zhang, W., J. Sloan-Lancaster, J. Kitchen, R.P. Trible, and L.E. Samelson. 1998. LAT: the ZAP-70 tyrosine kinase substrate that links T cell receptor to cellular activation. *Cell.* 92:83–92. https://doi.org/10.1016/S0092-8674(00)80901-0

Zhang, W., C.L. Sommers, D.N. Burshtyn, C.C. Stebbins, J.B. DeJarnette, R.P. Trible, A. Grinberg, H.C. Tsay, H.M. Jacobs, C.M. Kessler, et al. 1999. Essential role of LAT in T cell development. *Immunity.* 10:323–332. https://doi.org/10.1016/S1074-7613(00)80032-1

Zhou, B., Y. Wu, and X. Lin. 2011. Retromer regulates apical-basal polarity through recycling Crumbs. *Dev. Biol.* 360:87–95. https://doi.org/10.1016/j.ydbio.2011.09.009

Zou, Q., J. Jin, Y. Xiao, H. Hu, X. Zhou, Z. Jie, X. Xie, J.Y. Li, X. Cheng, and S.C. Sun. 2015. T cell development involves TRAF3IP3-mediated ERK signaling in the Golgi. *J. Exp. Med.* 212:1323–1336. https://doi.org/10.1084/jem.20150110